uc3m | Universidad Carlos III de Madrid

Bachelor Thesis

Degree in Aerospace Engineering

Preliminary design of an attitude control system for a high altitude platform

Daniel Sánchez-Biezma Zarco

Aerospace Engineering

Acknowledgements

The labor contained within this document has been supervised by Dr. Manuel Sanjurjo Rivo (Phd in Aerospace Engineering by Universidad Politécnica de Madrid) of the Department of Aerospace Engineering of Universidad Carlos III in Leganés. Without him this document would have never existed.

In addition I would like to express my most sincere gratitude to all the people that have shaped and gone with me during this journey that has been college. Thanks to Diego, Manuel, Adrian, Juan and Daniel who have been my faithful brothers in arms through this four years of hard work and studying.

Also thanks to Erika, Maria Jesus, David and Victor. My beloved friends in Pinto that encouraged me when I needed and with I spent the best moments of my life.

And finally. Thanks to my parents and family, who have raised me and turned me into the person I am.

Contents

List of Figures

List of Tables

1 Abstract

Within this document the process of developing different designs for the hardware of an attitude control system based on reaction wheels implemented in a high altitude platform is depicted along with a review of the most common attitude control systems used currently by different members of the aerospace industry.

The process consists mainly in three parts: First, developing a simulation environment that recreates the conditions in which the platform is expected to operate and implement the physical laws that govern the motion of these kind of artifacts, and is able to compute the geometrical characteristics of the different reaction wheels tested. Secondly the performance of different candidate designs of reaction wheels is tested and analyzed. And finally a selection between all these candidates is performed taking into account different elements like the time that each design takes to correct the attitude of the platform, the weight of the wheels, the required angular velocity to maintain the desired attitude and the cost of the material employed.

2 Socio-economic environment and impact of the project

Currently, many companies are willing to launch their own satellites for many goals like gather information from deep space or the surface of Earth, or provide communication services to their customers. Nonetheless, launching a kilogram of payload into space is currently about 20000 €, limiting dramatically the amount of mass that any entity can launch into space. In addition, the development of a satellite is a long, complex and expensive process that involves numerous branches of human knowledge and requires a lot of time and resources. Because of these reasons, small companies and autonomous entities like Universities are looking for cheaper alternatives like high altitude platforms or UAVs. Although the lifespan of these alternatives is much sorter (some days in the best conditions) than the life time of a satellite (which are in the interval of 5 to 50 years). In order to be able to achieve the goals mentioned before the control of the attitude is of paramount relevance. A flying platform not oriented in the optimal position can result in an ineffective transmission of data or the impossibility of collecting data such as images of a certain spot of Earth or space. However, these systems are be very expensive and sometimes they do not adjust properly to the requirements of their users since they are manufactured by other companies.

In order to avoid these problems, the development of hardware intended for attitude control system can be critical. This project, in which the process of the preliminary design of an attitude control system based on flywheels is depicted, could be used by the University or other entities that are aiming to launch a high altitude platform that requires an attitude control system. In addition, since this is a preliminary study, the ideas contained in this document could be further expanded and used to develop more precise and efficient reaction wheels.

By considering the design steps followed in this project the time and costs of designing and manufacturing the actuators for an attitude control system can be drastically reduced. In addition, an actuator can be specifically designed for each platform instead of having to buy one that surpass the requirements for controlling the platform, or one that is not capable to reach them. For instances, a reaction wheel capable of storing certain amount of torque that fits some required dimensions cannot be found in the market and must be ordered specifically, which usually increases the price of the product dramatically. In other words, actuators specially suited for a certain mission could be manufactured with the requirements desired at will by the user, without supposing a large amount in the cost of the actuator.

3 Introduction

3.1 Historical insight

Nowadays satellites are used to perform a wide variety of functions and task such as deep space and solar system observation, communications, Earth's surface inspection and spying among others.

These devices are composed by a numerous systems that allow the proper fulfillment of their objectives, communication system, power system or emergency systems are some of the many that can be found within these machines. Among all of them it is important to highlight the control system, which is in charge of leading the device into a desired state commanded by its operators or mission designers. The control system may be composed by many subsystems like the thermal control system, the position control system or the speed control system. There is in particular, a control subsystem of paramount relevance for missions regarding surveillance and equipment test missions, the attitude control system. This system is in charge of changing and/or maintaining a certain orientation commanded to the device in order to achieve an optimal state for many different goals like aiming to a certain spot on the ground to take a picture or orienting a satellite for its solar arrays to reach their maximum efficiency or even redirecting space debris during a launch in order to put them into a Earth-collision orbit with the goal of burning them in the atmosphere.

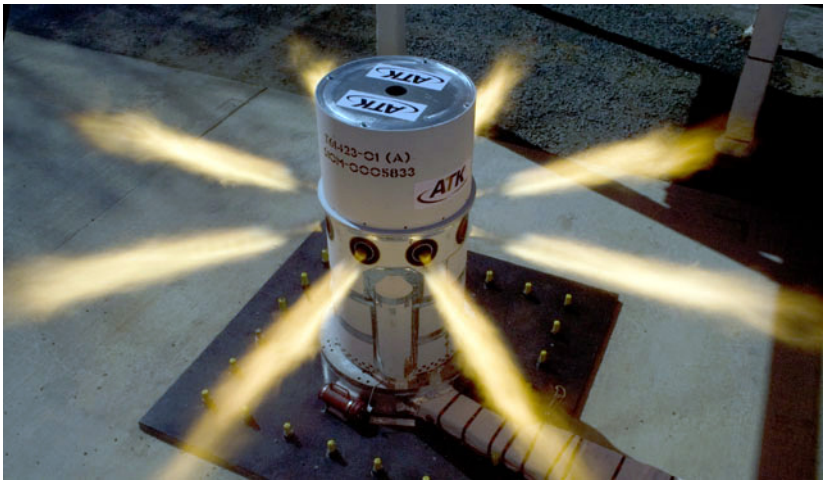

Figure 1: Attitude control system based on thrusters for a second Orion launch abort system developed by ATK being tested on ground.[1]

The use of attitude control system goes back in history to the first vehicles used by the mankind like carriages pulled by animals, then introduced in the first maritime vehicles like boats, leading to the ones employed in the first airplanes and space exploration devices.

One of the first attitude control devices developed by humans consisted in simple wooden steering wheels activated by levers that were capable of affecting the orientation of the carriage in which they were installed. These were later developed into the modern steering wheels used in cars and other ground vehicles. Nonetheless, there are other attitude control system for ground vehicles that are not based in steering wheels, like the counter rotating caterpillars used in tanks and other heavy vehicles.

The first elements used in maritime vehicles with the purpose of controlling their orientation consisted in elements that acted as hydrodynamic brakes that generated a torque that influenced the attitude of the vehicle and/or sails that oriented in a certain way took advantage of the wind to rotate the platform in which they were attached. These were later developed into the rudder-based systems that employ fins located at the backside of

the vehicle able to rotate and thus, inducing a moment about the center of mass of the vehicle in order to change the orientation of the vehicle. It is important to highlight that these fins are also hydrodynamic devices that only work if there is a flow passing by them. Finally with the implementation propellers that provide thrust to the vehicle, thrust vectoring could be also implemented and the orientation of the ship could be changed in a static state.

The first aerial vehicles like balloons had only altitude controls meaning that their orientation was dictated by wind and other external forces. Lately with the introduction of aircrafts with wings, devices that wrapped these parts of the aircraft were implemented. This wrapping changed the shape of the wings inducing and imbalance in the forces that acted on these surfaces generating a torque and subsequently a rotation. In low speed air vehicles like airships thrust vectoring propellers were used to modify their orientation. The next step consisted in the use of aerodynamic control surfaces located in different parts of the aircraft such as the tail and wings in order to provide the mentioned force imbalance to generate a rotation. Finally with the development of the jet engine thrust vectoring was made possible allowing airplanes to change its attitude at low speeds.

The first space vehicles that reached space used attitude control mechanism based on the control of the direction of the exhaust gases by means of vanes located at the nozzles since these vehicles were mainly rockets that were designed to reach a certain altitude and then fall back to Earth. Once orbital vehicles like satellites were developed other system where employed like attitude control by means of reaction wheels, thrusters and the interaction with the magnetic field of the planet as is explained in section 3.3.

It is important to highlight that the developments in the field of electronics allowed the implementation of unmanned controlled vehicles. Before these developments for a vehicle to be controlled it was compulsory to had a human acting on it from a relative close position leading to the impossibility of having fully controllable devices in orbit and deep space.

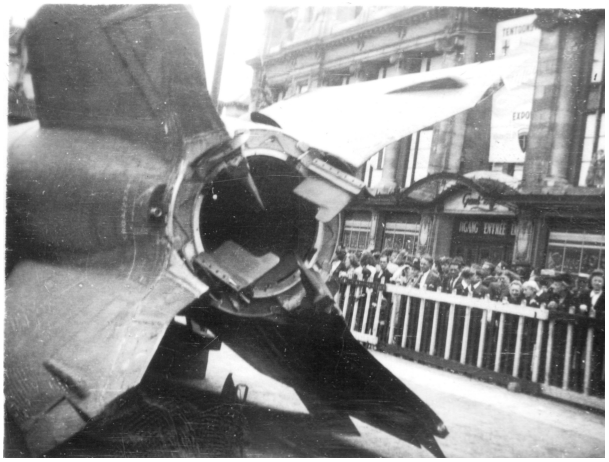

Figure 2: Exhaust vanes of a V-2 rocket developed by Nazi Germany. This rocket was the basis of the ones developed by the USA during the Space Race that took place in the second half of the XX Century[2]

3.2 Motivations and goals

The department of Bioengineering and Aerospace Engineering of University Carlos III is aiming in the direction of developing its own satellite and launching it. For that goal to be fulfilled, data from the high layers of the atmosphere is needed to be gathered, as well as to test different technologies and devices in environments that resemble LEO[1]conditions.

These tasks would be performed by a high altitude platform consisting in a balloon with a small platform to carry the experiments and different actuators. In addition to the science and techniques that this project would generate as a result, the students involved in this project will earn experience and gain new skills in different fields of aerospace engineering (such as fluid dynamics, Guidance Navigation and Control, mission planning and orbital mechanics) that would be essential for the future development of the satellite.

For this probe to perform its missions adequately an efficient and solid attitude control system is mandatory. This control system is the core that allows operations like aiming a camera into a certain spot on the surface of Earth or orientating the structure for a better data transmission. Nonetheless, the control system used in a certain platform must be properly selected or design in order to be able to allow that platform to operate properly and not losing control over its position and attitude.

One of the main disadvantages of the attitude control hardware based in torque storage currently employed in Cube-Sats[2] and high altitude platforms is that they are very expensive and may not be compatible with a control software that the University is familiarized with. For those reasons the idea of developing an attitude control system arose.

In order to design a complete attitude control system three fundamental parts are needed: A controller, actuators and sensors. Within this document it is spoken about all of these parts, nonetheless its main purpose is to depict the process of designing an actuator based in angular momentum storage (reaction wheel).

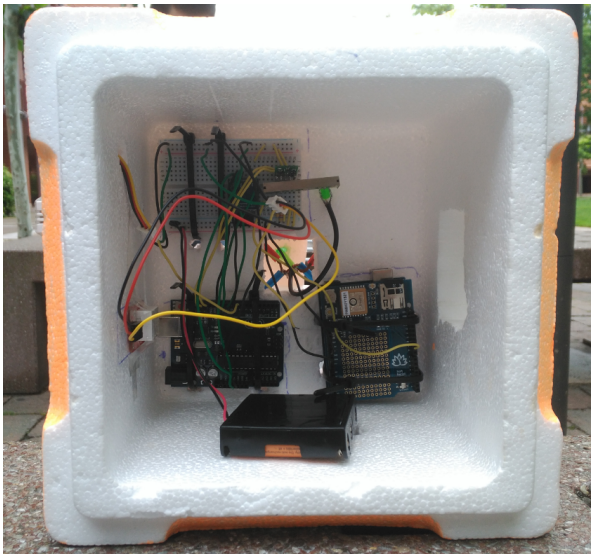

Figure 3: Insides of the developed by students of University Carlos III in which the attitude control system described within this document would be implemented

.

It is important to remark that the gondola in which the system is aimed to be installed is just a prototype, which means that the reaction wheels chosen as suitable at the end of this document may change with future changes in the project.

[1]Low Earth Orbit (LEO) are those orbits contained between 200 and 2000km of altitude, approximately until the first Van Allen radiation belt

[2]A cube-Sat is a kind of nano-satellite in which each edge is ten centimeters long and less than 1.33 kilograms of mass

3.3 State of the art

Since the last days of the Second World War many different systems for attitude control have been developed and implemented in different kind of devices such as bombs, rockets and satellites. These attitude control systems can vary in type being the most popular ones those that make use of thrusters, magnetic fields, aerodynamic actuators and reaction wheels. Each of the four systems is widely used depending on the requirements of the mission and the platform in which the attitude control is installed.

3.3.1 Actuators

3.3.1.1 Thrusters

Attitude control systems based on thrusters are most used in spacecrafts such as satellites and rockets. Due to the partial vacuum of orbital and interplanetary space aerodynamic actuators like ailerons or elevators are of no use since the lack of aerodynamic pressure renders them useless. Because of this situation, the only way of applying the third law of Newton to generate a change in attitude or position is by throwing away matter stored inside the platform, gaining some momentum in the opposite direction to the one in which the matter is throw away and generating some torque that allows the attitude modification of the platform. When torques are applied about each principal axis the platform falls in the category of three-axis stabilized. Nevertheless, this does not imply that a maneuver cannot be performed by applying a torque on each axis at a time. It is important to mention that these thrusters are located in opposite pairs and act coupled in such a way that the net force on the platform is zero.

This method of attitude control carries with it some advantages like the non-existence of saturation, a common disadvantage in reaction wheels. In addition this method is potentially the one that can provide the largest force on the spacecraft and also the largest torque. However it brings other disadvantages like the fact that it depends on the amount of propellant that it carries from the launch site. Once all the propellant is used the system becomes inoperative. Another disadvantage that comes along with the use of thrusters in spacecraft is sputtering. This phenomena arises when a cloud of particles of propellant gathers around the platform and litters the lenses of cameras, telescopes and others devices like antennas[5].

It may fall that for a spacecraft designed to have an extended lifetime, a combination of thrusters and reaction wheels could result in an optimal control system. The reaction wheels would propitiate the attitude control most of the time and the thrusters would eliminate the saturation caused by elements like solar wind and friction with the upper layer of the atmosphere. By this way, the usage of propellant would be minimized and the control of attitude can be maintained for longer than if only reaction wheels or thrusters alone were used.

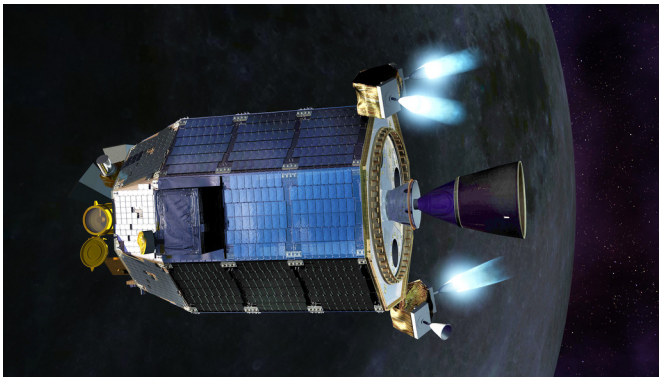

Figure 4: Computer design representation of attitude control thrusters in a satellite ejecting propellant during a maneuver[3].

3.3.1.2 Magnetic attitude control systems

This kind of attitude control system is mainly used by spacecrafts and rarely implemented in atmospheric vehicles due to the fact that the friction induced by the atmospheric gas is too strong for this sort of systems to be effective.

Magnetic attitude control systems operate by generating a magnetic field that interacts with the local magnetic field of the planet the spacecraft is orbiting. This effect can be seen as a compass trying to align with the magnetic north-south line of the magnetic field of the celestial body. The elements that make this attitude control possible are rod shaped electromagnets that creates a dipole when a current is applied through them. These artificial electromagnetic field tend to align with the magnetic field of Earth and since they are attached to the spacecraft the entire structure will follow that tendency. Their main advantage is that they only require electric power than can be obtained by means of photoelectric cells, which grant a long life span for the attitude control system. Also, the position of the center of mass is not altered using this kind of systems because no mass in the platform is altered. However, this method can only be applied for satellites located up to a certain distance from the planet their are orbiting due to the fact that the magnetic field of the celestial body decays strongly with distance. In addition, they cannot be used in equatorial orbits to avoid the north-south perturbation due to the fact that the north-south direction always lies in the horizontally. As a consequence, a spacecraft would not be able to correct any north-south disturbance.[5].

3.3.1.3 Gravity-gradient torque

Another technique used for attitude stabilization is the use of the reduction of the potential of gravity with height in order to maintain stability. Nevertheless, equilibrium can only be achieved if the axis with less inertia is aligned with the local vertical line. Furthermore the amount of torque that can be produced by means of this system is often very low.[5]

3.3.1.4 Aerodynamic actuators

This system is used mainly in atmospheric vehicles like planes, UAVs or balloons. Aerodynamic actuators make use of the pressure forces that arise when an object encounters a stream of fluid particles (because of the motion of the fluid in which the object is immersed, or due to the relative motion of the object in a static flow).

The torque generated by aerodynamic surfaces is highly dependent on the velocity of the stream and the effective area of the actuator as can be seen in equation 1, where F_a is the aerodynamic force, ρ the density of air, S the surface of the actuator and C_a the force coefficient dependent on the geometry of the aerodynamic surface.

$$F_a = \frac{1}{2}\rho V^2 S C_a \tag{1}$$

Following this expression it can be guessed that aerodynamic actuators are suitable for vehicles such as aircrafts and UAVs that move relatively fast and at low altitude where the density of air is greater. However, they can also be of used for high altitude platforms such as probe balloons as a measurement to counteract upcoming winds that can alter the attitude of the system.

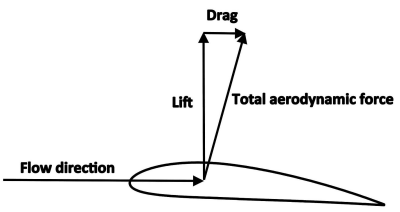

Figure 5: Aerodynamic force decomposition

The term C_a[3] is a parameter dependent on the geometry of the aerodynamic surface and the angle of attack. This coefficient is strongly related to the lift coefficient of the shape of the profile of the aerodynamic surface C_l. This coefficient is also strongly dependent on the geometric shape of the profile and the angle of attack. In terms of angle of attack it increases linearly for a range of small angle of attack with a slope of 2π. When the angle of attack is higher than the mentioned interval the boundary layer[4] is detached and lift generation is dramatically reduced as can be seen in figure 6.

There are two main kinds of aerodynamic profiles for aerodynamic surfaces: Cambered and uncambered. Cambered profiles are not symmetric and its shape enhances the generation of higher pressures in the lower part of the airfoil generating more lift for a certain angle of attack than an uncambered profile which are symmetric as can be seen in figure 6.

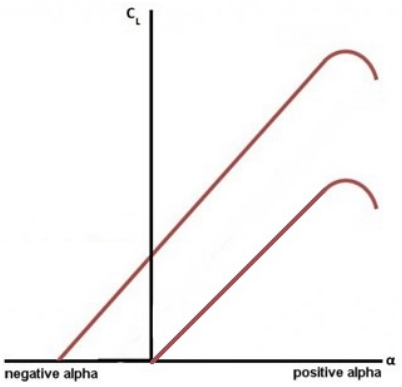

Figure 6: Lift slope of a cambered airfoil (upper) and a symmetric one (lower). As can be seen there is a region for high angles of attack where the boundary layer is detached and lift is no longer generated

Due the non symmetry of the cambered airfoils they are not useful for yaw control since lift is produced at zero angle of attack, leading to the generation of a force at neutral state inducing a permanent yaw in one direction.

3.3.1.5 Solar radiation pressure

Although in space the dynamic pressure exerted by a atmospheric gas on a spacecraft may tend to be zero, the pressure exerted by the light emitted by the sun is not negligible. This pressure arises due to the fact that light carries momentum and when it collides with a surface a momentum exchange occurs giving birth to solar radiation pressure. This is often seen as a problem in order to maintain a certain attitude state because it would tend to rotate the spacecraft in a certain way as a stream of gas would do in the atmosphere. Nonetheless this property of solar wind can be employed to correct the spacecraft orientation into a desired one[5].

The force that arises is no other than the vector difference between the momentum flux. The torque is the integration of the force over the illuminated area.

This method can be an efficient way to control the attitude of a body in space since it does not need to carry propellant and as long as the body is illuminated a solar pressure exists. However, this pressure decays with the distance to the star and the torque that is produced is very low, making it useful only for space vehicles relatively close to a star. In addition, large surfaces such as solar arrays are needed, compromising the total surface of the spacecraft[5].

All the methods seen so far take advantage of elements external to the spacecraft or aircraft, such as the Sun, the atmosphere or the magnetic field of a planet. Nonetheless there are other methods that do not make use of external agents and are based in the law of conservation of angular momentum.

[3]Lift coefficient.

[4]A very thin layer of the flow located very close to the walls of the airfoil where viscosity domains over inertial flow

3.3.1.6 Mass movement

One of the internal methods is mass movement. It consist in altering the position of the center of mass within the spacecraft or aircraft in order to change the tensor of inertia. This changes the balance of the body in a dynamic way affecting the torques caused by forces on the vehicle.

A way to alter the center of mass of a vehicle is by moving the fuel or propellant that it may carry. This method is used in aircrafts were fuel is transferred from one tank to another in order to ensure that the center of mass is ahead the neutral point[5].

3.3.1.7 Momentum storage torquers

These torquers are devices such as reaction wheels and momentum wheels (RWs and MWs respectively). They do not create or subtract any momentum form the platform, their function is to take advantage of the law of conservation of total angular momentum (equation 2)[5][5].

$$\frac{d\mathbf{H}_{total}}{dt} = \frac{d\mathbf{H}_{vehicle}}{dt} + \frac{d\mathbf{H}_{rotor}}{dt} = \mathbf{0} \tag{2}$$

Reaction wheels are designed as heavy disks with nominally zero rotational velocity. If a change in attitude is required they are force to rotate in a certain direction and speed changing its angular momentum in order to produce a change in the angular momentum of the vehicle resulting in a variation in attitude. This change is expected to be linear, however, due to sticking friction at low rotational speeds the relation is not often as expected. For that, the nominal speed is set slightly above of these nominal angular velocities[5].

On the other hand, momentum wheels are designed to have a high average rotational speed in order to provide momentum bias, which is the resistance of an axis to change its direction due to its higher momentum with respect the other axes[5].

Both kinds of systems require electric motors in order to perform their tasks. The ones for the momentum wheels must be designed to provide angular speeds in the interval of -10000 and 10000 rpm. Also momentum storage torquers are designed to have a life span of around fifteen years, so a very precise design and manufacturing with low tolerances are required.

In order to achieve total attitude control three wheels would be needed, each one located in one of the axis of the platform. Nonetheless, an rotating heavy wheel mounted in a gimbal can also be employed. The wheel would rotate at a constant rate while the gimbal would adapt in order to generate the required momentum bias. Their use its well extended in spacecraft and high altitude atmospheric platforms like balloons.

Despite the fact that no external means to the spacecraft are needed to control the attitude, two main problems arise within the use of these torquers. The first one is that the lifespan of the system is often too short for the mission. Usually the lifespan of a satellite is set around fifty years for high altitude orbits, which exceed the average lifespan of reaction and momentum wheels. The other problem is saturation due to friction with the upper layers of the atmosphere and solar radiation pressure. This problems arises when the spacecraft's attitude state is altered by dynamic pressure from air and light. This pressure forces the wheels to rotate at a certain speed in order to overcome the mentioned pressure. However, there is a point where the speed at which the wheels have to rotate to overcome the dynamic pressure exceed the limits of the motors. At this point an attitude control system based in momentum storage torquers is saturated and is no longer able to govern the orientation of the platform unless and external method is employed to remove the saturation. That is why a combination between external and internal system is widely used nowadays.

[5]Equation of conservation of the total angular momentum, where $\mathbf{H}_{total}$ stands for the total angular momentum of the system, $\mathbf{H}_{vehicle}$ for the angular momentum of the vehicle and $\mathbf{H}_{rotor}$ for the angular momentum of the reaction or momentum wheel

3.3.2 Attitude measurement (Sensors)

In order for a system to be a control system a way of measuring its current state is needed. For that reason a collection of techniques and instruments are used with the purpose of determining the attitude in a spacecraft or aircraft.

For this task two kinds of sensor devices are used and often in a way that they complement each other. These sensors are reference sensors and inertial sensors. The first ones gives a measure of the position of a fixed reference like the Sun or the Earth. While the latter ones measure changes in attitude relative to a gyroscope in a continuous way. In space there are some moments in which the reference position with respect to reference points as the Sun cannot be established due to interferences. Is in these moments where the inertial sensors measure the evolution of the motion of the spacecraft until the interferences disappear.

3.3.2.1 Star sensors

Star sensors take advantage of position of distant stars to determine the relative attitude of the platform in which they are mounted on. There are three kind of star sensors: Star scanners (used for spin stabilized spacecrafts), star trackers (used in three axis stabilized spacecrafts) and star mappers (also used in three axis stabilized spacecrafts). In the first one the rotation of the platform allows a scanning of a wide portion of the sky. By comparison of the stars "captured" by this scan the attitude can be determined. The second kind focus in a determined star with extreme precision, due to the fact that one star is not enough to determine attitude, two of these sensors are needed. Lastly, star mappers have a large FOV[6] that allows to capture and compare the position of multiple stars allowing a precise determination of attitude[5]-[4].

Figure 7: Star cameras used for the determination of attitude using the relative position of star in deep space. Baffles used to block light from lateral directions are missing leaving the cage exposed.[4]

[6]Field Of View

3.3.2.2 Sun sensors

These sensors are composed by a box with photo-sensors and a slit or pinhole in one side, as the light passes through this hole, the angle formed by the photon stream and the sensors is used to determine the attitude of the platform as can be seen in figure 8.[5]-[4]

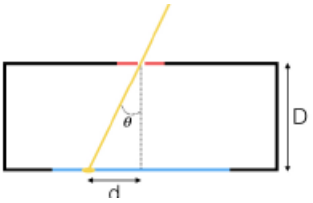

Figure 8: Light passing the pinhole of a sun sensor.[4]

3.3.2.3 Earth sensors

Earth sensors use images of Earth's horizon to determine the attitude of the platform in which they are installed. There are two main kinds of Earth sensors: Static Earth-horizon sensors are used for three axis stabilized spacecrafts in GEO[7], they keep an infrared image of earth between thermal sensors as can be seen in figure 9. Any change in attitude will change the position of this image with respect to the sensors leading to a change in their reading and thus the "acknowledgment" of a change in orientation. Scanning Earth-horizon sensors use a slit to scan the horizon in order to detect changes in the IR signal between Earth and deep space[5].

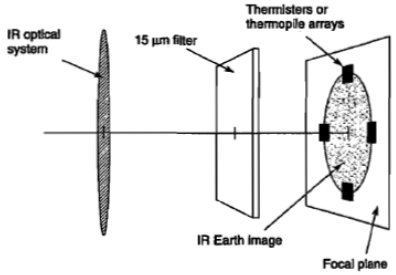

Figure 9: Static Earth-horizon sensor[5]

3.3.2.4 Magnetometers

Vehicles that perform missions in the vicinity of the magnetic field of a planet can use the natural orientation of the magnetic field lines (magnetic North-magnetic South) to calculate the relative attitude of the aircraft or spacecraft relative to the orientation of the magnetic field of the planet.

These magnetometers are devices that measure the amount of magnetic flux that goes through them. Following expression (3)[8], it can be stated that the flux is maximum when the magnetometer coil is aligned with the lines of magnetic field. While when these lines fall perpendicularly to the sensor the flux is null. By making use of 3 magnetometers the attitude of a vehicle can be easily determined. However, this system suffer from accuracy issues near the poles of a planet when the magnetic field variations are more pronounced[5].

$$\Phi = BAcos(\theta) \tag{3}$$

[7]Geostationary Orbit: Orbit with the property that any object in it will be always above the same point of the surface of Earth, i.e. the orbital velocity of a body located in such orbit is the same as the rotational velocity of Earth's surface in the Equator

[8]Equation for the magnetic flux where Φ is the magnetic flux, B is the intensity of the magnetic field, A the area of incidence of the lines of magnetic field and θ the angle of inclination of the area with respect to the lines of magnetic field

3.3.2.5 Global Navigation Satellite System (GNSS)

Although its main use is to determine the position of an object relative to the net of GPS satellites, attitude can also be determined by means of this system. This can be done using at least three antennas located along the direction of the three principal axes. Then, by analyzing the time difference between the moment when the signal emitted by the GPS is received in the set of antennas, the attitude of the platform relative to the satellite can be established. Nonetheless accuracy problems may arise since many GPS satellites can be emitting and multiple attitudes (relative to different GPS satellites) are obtained[5].

3.3.2.6 Inertial sensors

Inertial measurement of attitude is a "blind" method of determining the orientation of an object because it is not compared with any external reference. The most common type of inertial sensors for attitude are those based in the use of gyroscopes mounted on gimbals. The gimbal is attached to the platform frame, moving in concordance with the structure. The measure of the torque is performed with the angular rate about the sensitivity axis of the instrument as can be seen in equation (4) and figure 10.

A minimum number of three gyroscopes are needed in order to know the angular velocities about each axis $(\omega_x, \omega_y, \omega_z)$. For high precision systems gyroscopes with no moving parts are employed like Ring Laser Gyroscopes (RLG)[5].

$$\frac{d\psi}{dt} = \frac{T_N}{H} \tag{4}$$

By making use of equation (4)[9][6]. Once the variation of the angular speed of the gyroscope and its rate are known the torque and the change in attitude can be determined.

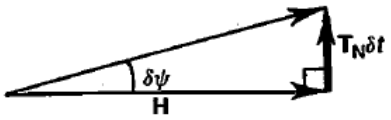

Figure 10: Precession induced a torque[6].

[9]Equation of the precession due to a torque T_N, being H the angular momentum and ψ the precession angle.

3.4 Controllers

Both the attitude control actuators and sensors cannot correct the orientation of an object by themselves. They are like the muscles and eyes of the attitude control system, but no system is complete without a brain. This brain is no other than the controller of the system.

A controller is a set of equations that governs the behavior of a system. A set of input parameters enter the equation and values of the same or other parameters exit it to be compared with the desired values (closed loop) or not (open loop). These, along with other variables like gains are the main elements of a controller.

The system of equations is often transformed into Laplace domain. This is made by means of the Laplace's Transform as can be seen in equation (5). The result of these process is known as transfer functions that are often represented as capital letters as can be seen in figure 11 In Laplace's domain the time dependent functions are transformed into frequency dependent ones, where s is a complex frequency parameter with a real part (amplitude) and an imaginary one (phase).

$$F(s) = \int_0^\infty f(t)e^{-st}dt \tag{5}$$

The system is then expressed in state-space representation in order to make it clearer and to ease the calculations as can be seen in equations (6) and (7)

$$\dot{x} = A(s)x(s) + B(s)u(s) \tag{6}$$

$$y = C(s)x(s) + D(s)u(s) \tag{7}$$

Where x is the state vector, A the system matrix, B the input matrix, u the input vector, y the output vector, C the output matrix and D the feed matrix.

3.4.1 Open Loop

As can be seen in figure 11, these controllers do not have a feedback that corrects the error of the output with respect to the desired values.

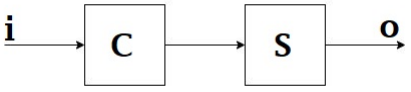

Figure 11: Simple representation of an open loop controller where i stands for input, o for output and C and S for controller and system respectively

These kind of controllers are only recommended for systems where the input and output are perfectly known and defined and not dependent on other environmental parameters. For instances, a controller that defines the temperature output of an electric resistance. Knowing the relations between the intensity of the current, the resistance and the temperature output, a certain temperature can be reached easily without "watching" real output value because it is already known. However, if we are interested in controlling the temperature of the room in which this resistance is located a controller that takes into account the output parameter and introduces it in the system is needed. These are closed loop controllers.

3.4.2 Closed Loop Controllers

As was mentioned before, closed loop controllers use the values of the output parameters as feedback in order to account for the error between the desired outputs and the actual ones.

The development of this controllers has been one of the most important technological milestones of the XX century, allowing the control of the outputs of a system with almost no error. The earliest closed loop controllers implemented the equations by means of analog techniques that were heavy and often impractical. However, in the fifties with the rise of digital controllers the true revolution began. Not only in aeronautics and other high technology fields, but also in domestic applications like the automatic speed controller of cars, the temperature output of ovens and other kitchen devices, even in the alarm clock there is a closed loop controller.

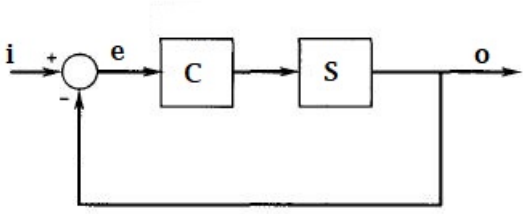

Figure 12: Simple representation of a closed loop controller

As was mentioned before, a controller is function that give a certain output values depending on the input values. For closed loop controllers there are three main kind of controllers: P (proportional), PI (proportional integral) or PID (proportional integral derivative) controller.

The P controller is a transfer function that multiplies $G_{\theta\delta_e}$ consisting in a constant value proportional to the error. In other words, the correction that it applies is proportional to the current difference between the commanded value and the actual output value. This kind of controller applies a very fast correction allowing the neutralization of the largest part of the error. However, its main drawback consists in the incapability of removing the steady state error with time.

The PI controller uses a combination between a proportional controller and a integral controller. The integral part analyzes the error over time and applies a correction based in the historic cumulative value of the difference between the output and the commanded value allowing the neutralization of the steady state error. However, despite being more complex than the proportional controller, its main drawback is the incapability of overriding the overshoot of the control.

In order to remove the problem with the overshoot in the PI, a derivative term D is added leading to the creation of a PID controller. This derivative term measures the rate of change of the response in time acting as an anticipating controller in such a way that the faster the rate of change of the error, the larger the correction applied will be.

$$P = k_p \tag{8}$$

$$PI = k_p + k_i \frac{1}{s} \tag{9}$$

$$PID = k_p + k_i \frac{1}{s} + k_d s \tag{10}$$

Expressions (8), (9) and (10) correspond to the expressions of P, PI and PID controllers, respectively. The k_p, $k_i \frac{1}{s}$ and $k_d s$ figures represent the proportional, integral and derivative terms.

The selection of the constants in expressions (8), (9) & (10) are selected depending on the requirements of the system. For instances, if little overshoot is desired a larger value of the derivative term would be used, or if a short time of response is necessary a large proportional term would be desirable.

4 Description of the high altitude platform

Before diving into the definition of the main activities developed it is of paramount relevance to illustrate the reader about the platform in which the attitude control system would be installed.

The overall system would be composed by a helium balloon and a small gondola. The balloon is in charge of lifting the gondola up to an approximate altitude of 30000 meters where it is expected to explode and fall back to the ground. The gondola is a small prismatic box made of expanded polystyrene in which all the sensors, tracking and communication equipment is installed. The dimensions of this box are 22 centimeters wide, 22 centimeters deep and 19 centimeters in height with a wall thickness of 3 centimeters. The mass of this platform is around 1.7 kg which allows the use of light reaction wheels.

The gondola and the balloon would be joined by a hinged system that would allow the independent rotation of each part with respect to the other part. Also, the length of the string that join both parts shall be short enough to avoid high amplitude and long period pendulum motion of the platform that takes long time to dissipate due to the perturbations generated by gusts and other external elements.

In addition, an experimental parachute system would be implemented in the platform in order to avoid potential damage dealt to the gondola and its internal components by a collision at high speeds with the ground.

Figure 13: Rough depiction of the final Balloon-Platform system made with CAD software

5 Methodology

Within this section the procedures and tools used to recreated a simulation environment in order to test the performance of the different hardware alternatives are described as well as the physics and mathematics involved in this kind of analysis.

5.1 Software

The simulation environment was developed using different computer softwares such as MATLAB and Simulink.

Furthermore, CAD models of the wheel designs were made in order to provide some insight of how these candidates are. The software in which these designs were created is Dassault Systemes CATIA V5. In addition, many different inertial properties were obtained by means of this program due to the complex shape of some alternatives that made cumbersome the resolution of the mentioned properties by conventional ways, such as the tensor of inertia or the volume.

5.2 Mathematics, physics and simulation Environment

Because testing the different alternatives for the attitude control system in real life requires a lot of time, effort and resources, a simulation environment in MATLAB and Simulink was developed in order to estimate how these distinct candidates perform and which one is the optimal for the project.

This environment was built up by means of the physics and mathematics involving attitude mechanics for the possible actuators that could be used for the control system. Before giving the reader more details about the simulation environment, it is important to give some insight about the science involved in it.

5.2.1 Attitude Kinematics

The definition of attitude makes reference to the angular orientation of an object in space with respect to a reference frame considered fixed. Currently there are many methods for expressing attitude in the realm of mathematics. Nonetheless, the methods employed in the development of this project were two: Euler angles and quaternions.

5.2.1.1 Euler angles

This method defines three main attitude angles for rotations. These angles are ϕ for rotations about the x-axis, θ for rotations about the y-axis and ψ for rotations about the z-axis, although this notations may change depending on the author of the document. These are the Euler angles and their main property is that an attitude state can be defined as a sequence of rotations about the initial reference frame considered fixed.

For instances, picture a vector **P** composed by its three components $P_x\mathbf{i}$, $P_y\mathbf{j}$ and $P_z\mathbf{k}$, and its components after a rotation with respect to the reference frame $P'_x\mathbf{i'}$, $P'_y\mathbf{j'}$ and $P'_z\mathbf{k'}$. It can be stated that:

$$\mathbf{P} = P_x\mathbf{i} + P_y\mathbf{j} + P_z\mathbf{k} = P'_x\mathbf{i'} + P'_y\mathbf{j'} + P'_z\mathbf{k'} \tag{11}$$

Which can be written in matrix form as:

$$(\mathbf{i} \quad \mathbf{j} \quad \mathbf{k}) \begin{Bmatrix} A_x \\ A_y \\ A_z \end{Bmatrix} = (\mathbf{i'} \quad \mathbf{j'} \quad \mathbf{k'}) \begin{Bmatrix} A_{x'} \\ A_{y'} \\ A_{z'} \end{Bmatrix} \tag{12}$$

That can also be expressed as:

$$\begin{Bmatrix} A_{x'} \\ A_{y'} \\ A_{z'} \end{Bmatrix} = \begin{pmatrix} \mathbf{i'} \cdot \mathbf{i} & \mathbf{i'} \cdot \mathbf{j} & \mathbf{i'} \cdot \mathbf{k} \\ \mathbf{j'} \cdot \mathbf{i} & \mathbf{j'} \cdot \mathbf{j} & \mathbf{j'} \cdot \mathbf{k} \\ \mathbf{k'} \cdot \mathbf{i} & \mathbf{k'} \cdot \mathbf{j} & \mathbf{k'} \cdot \mathbf{k} \end{pmatrix} \begin{Bmatrix} A_x \\ A_y \\ A_z \end{Bmatrix} \tag{13}$$

Leading to the simplified expression:

$$\begin{Bmatrix} A_{x'} \\ A_{y'} \\ A_{z'} \end{Bmatrix} = C \begin{Bmatrix} A_x \\ A_y \\ A_z \end{Bmatrix} \tag{14}$$

Where C is the so called rotation matrix. By inspection of the previous expression it can be stated that any rotation of a vector can be performed by multiplying the current state by the proper rotation matrix. In addition, this problem can be taken one step further and it can be said that any rotation can be represented by an axis (Euler axis) and an angle of rotation about that axis (principal angle). This axis can be found by taking the first eigenvector of the rotation matrix, while the angle is obtained by means of equation 15 where the trace of matrix **C** is the sum of its eigenvalues[6].

$$\Phi = arcos\left(\frac{1}{2}\left(trace\mathbf{C} - 1\right)\right) \tag{15}$$

Once these terms have been clarified a deeper insight in Euler angles can be made. Following the line of the rotation matrix it can be stated that if a single rotation of a vector about a reference frame can be expressed by means of a matrix, also can a sequence of rotations. Firstly, it is important to mention that the final state of a sequence of rotations is highly dependent on the order in which these rotations take place. This means that the result of rotating and object 45º about its x-axis clockwise, then 90º about it y-axis counter clockwise and finally 30º about its z-axis clockwise would not be the same as doing the same steps but in different order. There are many ways of expressing an attitude state with a sequence of rotations. Nonetheless, one of the most common sequences and the one used in this project is the $(\psi)_3$, $(\theta)_2$ & $(\psi)_1$ sequence that can be seem in figure 14. This sequence consist in a rotation of an angle ψ about the Z-axis, the a rotation of θ angles about the Y'-axis and finally a rotation of ψ angles about the X"-axis, all of them counterclockwise.

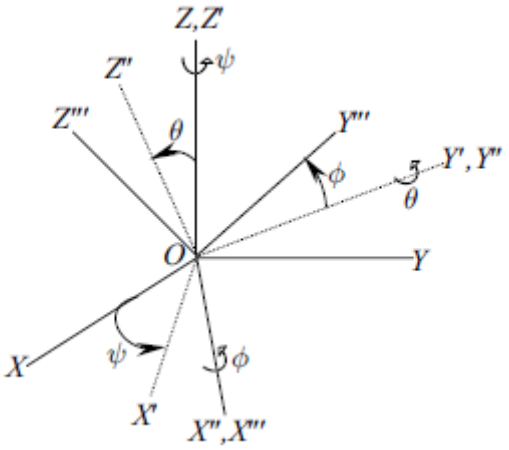

Figure 14: $(\psi)_3$, $(\theta)_2$ & $(\psi)_1$ rotation sequence.
[6]

Being the simplified mathematical representation:

$$C = C_1(\psi)C_2(\theta)C_3(\psi) \tag{16}$$

Being the result of the product the one depicted in expression 17.

$$C = \begin{pmatrix} cos(\theta)cos(\psi) & cos(\theta)sin(\psi) & -sin(\theta) \\ sin(\phi)sin(\theta)cos(\psi) - cos(\phi)sin(psi) & sin(\phi)sin(\theta)sin(\psi) + cos(\phi)cos(\psi) & sin(\phi)cos(\theta) \\ cos(\phi)sin(\theta)cos(\psi) + sin(\phi)sin(\psi) & cos(\phi)sin(\theta)sin(\psi) - sin(\phi)cos(\psi) & cos(\phi)cos(\theta) \end{pmatrix} \tag{17}$$

In order to obtain the Euler angles from the $(\psi)_3$, $(\theta)_2$ & $(\psi)_1$ representation the inverse transformations depicted in expressions (18), (19) and (20), where the sub indexes of c are the row and column of the element of the matrix.

$$\phi = tan^{-1}\left(\frac{c_{23}}{c_{33}}\right) \tag{18}$$

$$\theta = -sin^{-1}\left(c_{13}\right) \tag{19}$$

$$\psi = tan^{-1}\left(\frac{c_{12}}{c_{11}}\right) \tag{20}$$

However, this method presents two major drawbacks. The first one is that the angles obtained from the previous expressions are not unique. In other words, they may take different values for angles that share the same sin, cos or tan. The other major drawback is that for certain orientations like $(\psi)_3$, $(90^o)_2$ and $(\psi)_1$ a singularity appears. In these cases the representation is said to be singular and becomes useless. In order to avoid this situation another representation can be chosen. Nonetheless, this new orientation will have singularities at other orientations. Because of this problem Euler angles cannot be used to represent the attitude of systems that can present arbitrary orientation. To do that, a representation that uses four elements is needed.

5.2.1.2 Quaternion representation

This representation is derived from the Euler axis and principal angle representation, and has no singularities. A quaternion is a set of four scalar parameters, three of them form a vector called vector part and the other one the scalar part. These elements can be obtained directly from the Euler axis and principal angle:

$$q_{1,2,3} = e_{1,2,3}sin\left(\frac{\Phi}{2}\right) \tag{21}$$

$$q_4 = cos\left(\frac{\Phi}{2}\right) \tag{22}$$

Where the $q_{1,2,3}$ stand for the three different components of the vector part and $e_{1,2,3}$ the different components of the Euler axis.

One fundamental property that can be derived from the expression above is that:

$$q_1^2 + q_2^2 + q_3^2 + q_4^2 = 1 \tag{23}$$

From expression (23) it can be stated that a quaternion is composed by three independent elements (q_1, q_2 & q_3) and a fourth element that fulfills the equation. A quaternion defines a four dimensional space and it can be said that any attitude orientation lies and varies on the surface of a four dimensional sphere with no singularities. A simpler way to understand this is by imaging the set of components of the quaternion as a complex space, similar to the classic bi-dimensional complex plane, but composed by three complex vectors (q_1, q_2 & q_3) and a real one (q_4)[6].

Apart from the advantage of having no singularities. It is important to highlight that no complex trigonometric operations are needed when dealing with this kind of representation. This makes the quaternion method a more efficient way of expressing and calculating attitude for computer, requiring less operations than Euler angles representation. Nonetheless, it is needed to transform the quaternion into a rotation matrix in order to know the final angular values of the attitude. These changes of representation are depicted in expressions (24) and (25), (26), (27) and (28).

$$C = \begin{pmatrix} q_1^2 - q_2^2 - q_3^2 + q_4^2 & 2\left(q_1 q_2 + q_3 q_4\right) & 2\left(q_1 q_3 - q_2 q_4\right) \\ 2\left(q_1 q_2 - q_3 q_4\right) & -q_1^2 + q_2^2 - q_3^2 + q_4^2 & 2\left(q_2 q_3 + q_1 q_4\right) \\ 2\left(q_1 q_3 + q_2 q_4\right) & 2\left(q_2 q_3 - q_1 q_4\right) & -q_1^2 - q_2^2 + q_3^2 + q_4^2 \end{pmatrix} \tag{24}$$

$$q_1 = \frac{c_{23} - c_{32}}{4q_4} \tag{25}$$

$$q_2 = \frac{c_{31} - c_{13}}{4q_4} \tag{26}$$

$$q_3 = \frac{c_{12} - c_{21}}{4q_4} \tag{27}$$

$$q_4 = \pm\sqrt{1 + trace\mathbf{C}} \tag{28}$$

Another important advantage of quaternion representation is that a sequence of rotations can be expressed by the called composition rule:

$$\begin{Bmatrix} q_{1_2} \\ q_{2_2} \\ q_{3_2} \\ q_{4_2} \end{Bmatrix} = \begin{pmatrix} q_{4_1} & q_{3_1} & -q_{2_1} & q_{1_1} \\ -q_{3_1} & q_{4_1} & q_{1_1} & q_{2_1} \\ q_{2_1} & -q_{1_1} & q_{4_1} & q_{3_1} \\ -q_{1_1} & -q_{2_1} & -q_{3_1} & q_{4_1} \end{pmatrix} \begin{Bmatrix} q_{1_0} \\ q_{2_0} \\ q_{3_0} \\ q_{4_0} \end{Bmatrix} \tag{29}$$

Where the sub-indexes 0,1 and 2 stand for the original state, the rotation induced and the final state respectively. It can be seen that only 16 multiplications are needed instead of the 27 needed with rotation matrices. Another important property of quaternions is that they can be derived in time by means of the following expression:

$$\frac{d\left(\mathbf{q}, q_4\right)^T}{dt} = \frac{1}{2}\Omega\left(\mathbf{q}(t), q_4\right)^T \tag{30}$$

Where Ω is the skew matrix of angular velocities:

$$\Omega = \begin{pmatrix} 0 & w_z & -w_y & w_x \\ -w_z & 0 & w_x & w_y \\ w_y & -w_x & 0 & w_z \\ -w_x & -w_y & -w_z & 0 \end{pmatrix} \tag{31}$$

5.2.2 Attitude Dynamics

Controlling the attitude of an object requires to exert a force in order change the current its current state as Newton's first law of motion dictates[10]. When this force is not applied directly on the center of mass of the object a torque is produced as a result. In equations (32)[6] and (33)[6] the expressions for the total torque that a body experiences are depicted as a sum of all the forces applied in all the mass points and in integral form respectively, where $\mathbf{M}$ is the momentum, $\mathbf{r}$ is the distance between a point and the center of mass of the object, ∂m the infinitesimal of mass and $\frac{d\mathbf{v}}{dt}$ the acceleration of the infinitesimal mass point.

$$\mathbf{M} = \sum \left(\mathbf{r} \times \partial m \frac{d\mathbf{v}}{dt} \right) \tag{32}$$

$$\mathbf{M} = \int \left(\mathbf{r} \times \frac{d\mathbf{v}}{dt} \right) dm \tag{33}$$

Another important element that is needed to be taken into account is the angular momentum. Angular momentum is the equivalent of the linear momentum but for rotative motion. It is represented as the integral of the vector product between the distance of a mass point to the center of mass and the velocity of that mass point times the differential of mass.

$$\mathbf{H} = \int \mathbf{r} \times \mathbf{v} dm \tag{34}$$

It is of paramount importance to highlight that momentum is the time derivative of the angular momentum as can be seen in equations (35)[6] and (36)[6].

$$\frac{d\mathbf{H}}{dt} = \int \mathbf{v} \times \mathbf{v} dm + \int \mathbf{r} \times \frac{d\mathbf{v}}{dt} dm \tag{35}$$

$$\frac{d\mathbf{H}}{dt} = \mathbf{M} \tag{36}$$

Note that in the upper expressions the distance between the point and the center of mass is considered variable. Nonetheless, in the cases studied within this project the different actuators analyzed are assumed rigid enough for them to be considered as rigid bodies. Because of this condition the distance between a point and the center of mass is treated as a constant. With this fact in mind the velocity of a point if a body can be expressed as in expression (37)[6].

$$\mathbf{v} = \mathbf{v}_p + \omega \times \mathbf{r} \tag{37}$$

Introducing this into the angular momentum expression renders:

$$\mathbf{H} = \int \mathbf{r} \times \mathbf{v}_p dm + \int \mathbf{r} \times (\omega \times \mathbf{r}) \, dm \tag{38}$$

Finally leading to:

$$\mathbf{H} = \int \mathbf{r} \times (\omega \times \mathbf{r}) \, dm \tag{39}$$

Where *omega* is the angular velocity of the reference frame and $\mathbf{v}_p$ the velocity of velocity if the center of mass. By expressing $\mathbf{r}$ as the sum of its vector components the angular momentum can be finally expressed as:

$$\mathbf{H} = \mathbf{I}\omega \tag{40}$$

[10] Newton's first law of motion states that a body with mass remains in its current state unless a force is applied to it.

Where I is the tensor of inertia as depicted in equation (41). It is important to mention that the elements located in the diagonal of the matrix are called moments of inertia, while the other terms receive the name of products of inertia.

$$I = \begin{pmatrix} \int \left(y^2 + z^2\right) dm & -\int xydm & -\int xzdm \\ -\int xydm & \int \left(x^2 + z^2\right) dm & -\int yzdm \\ -\int xzdn & -\int yzdm & \int \left(x^2 + y^2\right) \end{pmatrix} \tag{41}$$

The values inside the tensor of inertia may be cumbersome to obtain and time varying for most of the cases. Nonetheless, exist a set of axis which maintain those values constant and furthermore makes the products of inertia equal to zero. In addition, by making this axes fixed to the body it is possible to make ω constant. These are called the body fixed principal axes.

Finally, taking all of these into account and working with expression (36)[6] it can be said that:

$$\mathbf{T} = \mathbf{I}\frac{\partial \omega}{\partial t} + S\left(\omega\right)\mathbf{J}\omega \tag{42}$$

Where $S(\omega)$ is the skew-matrix of the angular velocity.

$$S\left(\omega\right) = \begin{pmatrix} 0 & -\omega_z & \omega_y \\ \omega_z & 0 & -\omega_x \\ -\omega_y & \omega_x & 0 \end{pmatrix} \tag{43}$$

5.2.3 Longitudinal Dynamics

Due to the fact that during its operation the platform in which the control system is going to be mounted is not going to experience forces capable of deforming it, a rigid body model can be applied to describe its motion.

The nominal orientation of the platform is the one that has the z-axis in the direction of the weight pointing away from the center of Earth, and the x-axis and y-axis forming a perpendicular plane to the z-axis. Being their angles and angular velocities ϕ and ω_x or p (for the x-axis), θ and ω_y or q (for the y-axis), and ψ and ω_z or r (for the z-axis). Since the different components of the angular velocity are the derivative of their respective angles, the relation between them can be depicted as:

$$\begin{bmatrix} p \\ q \\ r \end{bmatrix} = \mathbf{K} \begin{bmatrix} \dot{\phi} \\ \dot{\theta} \\ \dot{\psi} \end{bmatrix} \tag{44}$$

Being **K** equal to:

$$\mathbf{K} = \begin{pmatrix} 1 & 0 & -sin(\theta) \\ 0 & cos(\phi) & sin(\phi)cos(\theta) \\ 0 & -sin(\phi) & cos(\phi)cos(\theta) \end{pmatrix} \tag{45}$$

The inverse relation gives the following expression.

$$\begin{bmatrix} \dot{\phi} \\ \dot{\theta} \\ \dot{\psi} \end{bmatrix} = \mathbf{K}^{-1} \begin{bmatrix} p \\ q \\ r \end{bmatrix} \tag{46}$$

The forces experienced by the platform can be described departing from Newton's second law.

$$\mathbf{F}_{pl} = m_{pl}\dot{V_{pl}} \tag{47}$$

Where $\mathbf{F}_{pl}$, $\dot{V_{pl}}$ are the vectors of the force and acceleration experimented by the platform and m_{pl} its mass. Where V_{pl} is composed by u,v and w, which are the three velocity components of the platform with respect to the Earth frame in the x, y and z-axes respectively. The previous equation expressed in the Earth frame turns out to be:

$$\mathbf{F}_{pl} = m_{pl}\left(\dot{V_{pl}} + \omega_{pl} \times V_{pl}\right) \tag{48}$$

Where ω_{pl} is the angular velocity of the platform.

The force experienced by the platform is the result of the action of gravity and the wind as expression (49) states:

$$\mathbf{F}_{pl} = m_{pl}\mathbf{C}\begin{bmatrix}0\\0\\g\end{bmatrix}\begin{bmatrix}X\\Y\\Z\end{bmatrix} \tag{49}$$

Where $\mathbf{C}$ is the rotation matrix, g the value of the gravitational field and X, Y and Z the aerodynamic forces in their respective directions. Finally, by developing the previous expression the following three equations can be obtained for the forces experienced by the platform.

$$(\dot{u} + qw - rv) = \frac{X}{m} - gsin(\theta) \tag{50}$$

$$(\dot{v} + ru - pw) = \frac{Y}{m} + gcos(\theta)sin(\phi) \tag{51}$$

$$(\dot{w} + pv - qu) = \frac{Z}{m} + gcos(\theta)cos(\phi) \tag{52}$$

The position of the system in Euler angle representation can be represented as:

$$\begin{bmatrix}\dot{x}\\\dot{y}\\\dot{z}\end{bmatrix} = C^{-1}V_{pl} \tag{53}$$

Which lead to the expressions (54)[7], (55)[7] and (56)[7].

$$\dot{x} = ucos(\theta)cos(\psi) + v\left(sin(\phi)sin(\theta)cos(\psi) - cos(\phi)sin(\psi)\right) + w\left(cos(\phi)sin(\theta)cos(\psi) + sin(\phi)sin(\psi)\right) \tag{54}$$

$$\dot{y} = ucos(\theta)sin(\psi) + v\left(sin(\phi)sin(\theta)sin(\phi) + cos(\phi)cos(\psi)\right) + w\left(cos(\phi)sin(\theta)sin(\psi) - sin(\phi)cos(\psi)\right) \tag{55}$$

$$\dot{z} = -usin(\theta) + vsin(\phi)cos(\theta) + wcos(\phi)cos(\theta) \tag{56}$$

5.2.4 Reaction Wheels

As was mentioned in the section 3.3.1.7, these devices take advantage of the law of conservation of angular momentum, generating changes in the angular velocity and attitude of the platform by changing their own angular velocity.

Departing from expressions (2) and (40) the following expression can be obtained:

$$\frac{d\mathbf{H}_{pl}}{dt} = \left(\mathbf{I}_{pl} + \mathbf{I}_r\right)\frac{d\omega_{pl}}{dt} + \frac{d\mathbf{I}_{pl}}{dt}\omega_{pl} + \mathbf{I}_r\frac{d\omega_r}{dt} + \frac{d\mathbf{I}_r}{dt}\omega_r \tag{57}$$

Nonetheless, expression (57)[6] is related to body axes. Taking the derivative with respect to the Earth's reference system expression (58)[6] is obtained.

$$\frac{\partial \mathbf{H}_{pl}}{\partial t} = -\mathbf{I}_r \left(\frac{\partial \left(\omega_{pl} + \omega_r \right)}{\partial t} + S\left(\omega_{pl} \right) \omega_r \right) - S\left(\omega_{pl} + \omega_r \right) \mathbf{I}_r \left(\omega_{pl} + \omega_r \right) - \mathbf{I}_{pl} \frac{\partial \omega_{pl}}{\partial t} + S\left(\omega_{pl} \right) \mathbf{I}_{pl} \omega_{pl} \tag{58}$$

As can be seen in expression (58) there are two main components in the right hand side of the equation, one related with the variation in angular momentum caused by the reaction wheels and other related with the variation given by the platform itself.

In the same way as in expression (40) the torque generated by a reaction wheel can be represented as:

$$\mathbf{T}_r = \mathbf{I}_r \frac{\partial \omega_r}{\partial t} + S\left(\omega_r \right) \mathbf{I}_r \omega_r \tag{59}$$

Due to the fact that the platform in which the control system is going to be used is a gondola attached to a balloon the main attitude parameters to control are the rotation angle about the vertical axis and its related angular speed[11]. Since only the motion about one axis is needed to be controlled a single reaction wheel would be enough.

In order to test the effectiveness of different designs of reaction wheels for the system, a controller was implemented in the simulation environment. With it, the performance of reaction wheels with different mass distributions, sizes and densities is tested, being the most optimal design the one that offers the best balance between control effectiveness and price and manufacturing difficulty.

The controller would be a PID controller with one feedback, the azimuth angle ψ. It can be seen in equation (46) that only controlling the azimuth angle its related angular velocity can also be controlled.

The current value of the azimuthal angle feeds the is compared with a commanded value for that angle. The difference between these two values (error) feeds the controller which sends a required torque that the reaction wheel must output. With this value of the torque the required variation of the angular velocity of the reaction wheel is calculated and with it the resultant variation of the angular speed of the platform and the new azimuth angle. Before continuing with the description of the problem it is important to highlight that the body axes of the platform are chosen to be the principal axes in such a way that the products of inertia ($I_{xy}, I_{yx}, I_{xz}, I_{zx}, I_{yz}, I_{zy}$) are zero. In addition the reaction wheel is meant to be placed in such a way that its z-axis is aligned with the one of the platform in order to provide a better control of the platform. It also has to be said that this two axis must be coincident with the center of mass of the system.

The physical model of the balloon and gondola was validated by means of some data of an actual fly of a very similar platform courtesy of the Center of Aerospace Development of the National Institute of Technology of Mexico. The information contained within this data included measurements of the acceleration and the angular velocity of the gondola. In order to obtain the attitude, external torque, forces and velocities some calculations had to be performed.

The angular acceleration was obtained by discrete derivation of the mentioned sample. Forward derivation was used for the first value of the angular acceleration while backward derivation and mean derivation was used for the last and the rest of the values respectively, where t stands for the time of an n value.

$$\alpha_n = \frac{\omega_{n+1} - \omega_n}{t_{n+1} - t_n} \tag{60}$$

$$\alpha_n = \frac{\omega_{n+1} - \omega_{n-1}}{t_{n+1} - t_{n-1}} \tag{61}$$

$$\alpha_n = \frac{\omega_n - \omega_{n-1}}{t_n - t_{n-1}} \tag{62}$$

[11] The axis with the same direction as the weight force, pointing away from the center of Earth.

For the calculation of the torque experienced by the gondola the following expression was employed.

$$T = I\alpha \tag{63}$$

Where I and α are the mass and angular velocity of the gondola. Despite the fact that the final goal is to implement the attitude control system into a hypothetical cube-sat developed by the University in the future. The gondola in which the attitude control system would be implemented preliminarily consists in a light box of 22 centimeters wide, 22 centimeters deep and 19 centimeters in height. The box width of the box's walls is x millimeters. The empty mass of this gondola is y kilograms and its tensor of inertia can be obtained by expressions (64)[8], (65)[8] and (66)[8], where A, B, H, a, b and h are the width, the depth and the height of the external and internal walls respectively.

$$I_{xx} = \frac{1}{12}m\left(B^2 + H^2\right) - \frac{1}{12}m\left(b^2 + h^2\right) \tag{64}$$

$$I_{yy} = \frac{1}{12}m\left(A^2 + H^2\right) - \frac{1}{12}m\left(a^2 + h^2\right) \tag{65}$$

$$I_{zz} = \frac{1}{12}m\left(A^2 + B^2\right) - \frac{1}{12}m\left(a^2 + b^2\right) \tag{66}$$

Finally for the force the second law of Newton was applied and for the velocity and the attitude a discrete integration of the acceleration and the angular velocity respectively was performed as can be seen in expressions (67) and (68).

$$v_n = \sum \left(a_n - a_0\right)\Delta t \tag{67}$$

$$\begin{bmatrix}\phi\\ \theta\\ \psi\end{bmatrix} = \sum \left(\begin{bmatrix}\omega_{xn}\\ \omega_{yn}\\ \omega_{zn}\end{bmatrix} - \begin{bmatrix}\omega_{x0}\\ \omega_{y0}\\ \omega_{z0}\end{bmatrix} \right) \Delta t \tag{68}$$

Where a, and Δt stand for the longitudinal acceleration and the time step of the data sample respectively.

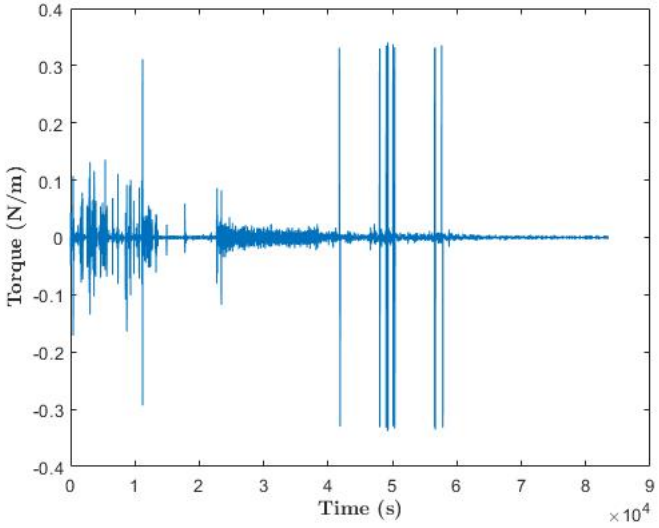

Figure 15: Spectrum of the torque obtained after provided data of angular velocity

The angular velocity and acceleration where recalculated using the physical model developed for the simulation giving the results that can be seen in figures 16 and 18. In the first one little difference between the original and processed values can be appreciated. Nonetheless, the angular velocity present certain degree of dissimilarity due to the fact that the tensor of inertia of the gondola was computed from some measurements provided by the aforementioned institution that only allowed a rough approximation of this parameter.

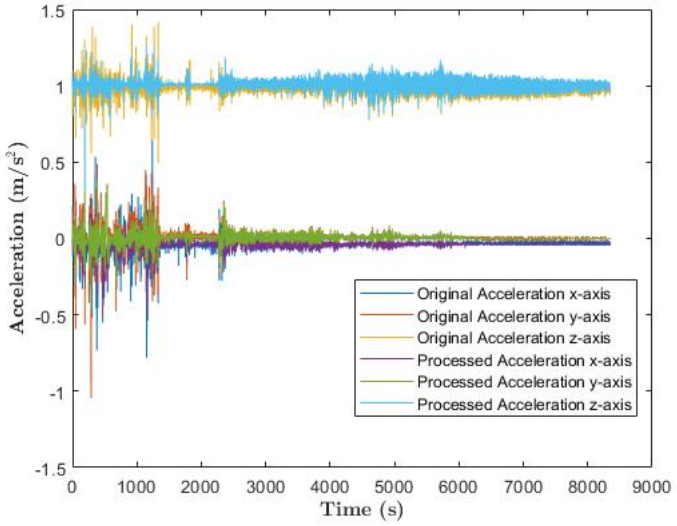

Figure 16: Comparison between the acceleration obtained by direct measurements and the processed one.

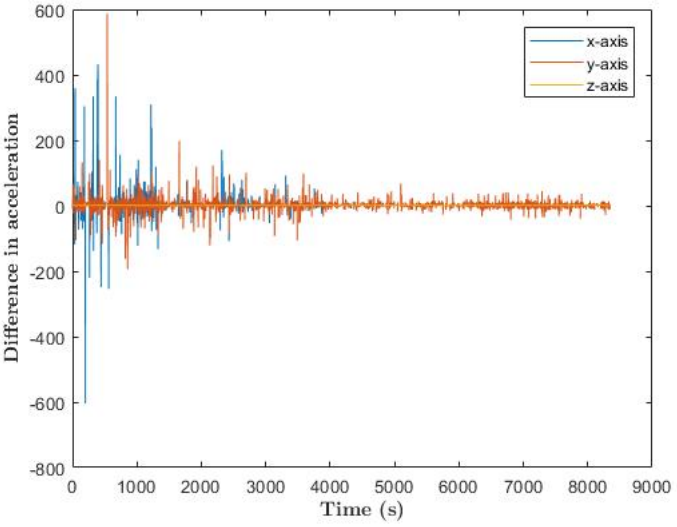

Figure 17: Difference between the original values and the processed ones.

The kind of reaction wheel that is going to be studied in this document is a compact design than is going to be compared to a lighter design of similar dimensions.

- Compact wheels are modeled as heavy wheel composed by two parts consisting in a ring joined to an electric motor by a rod. The two parts that compose the wheel are solid and isotropic pieces without irregularities.

  In order to compute the diagonal terms of the tensor of inertia of the three elements of the reaction wheels

the terms of expression (41 were employed).

Due to the fact that the arm is modeled as a solid cylinder equations (69)[9], (70)[9] and (71)[9] are used to determine its inertial properties.

$$I_{xx} = \frac{1}{12} m \left(3r^2 + h^2\right) \tag{69}$$

$$I_{yy} = \frac{1}{12} m \left(3r^2 + h^2\right) \tag{70}$$

$$I_{zz} = \frac{1}{2} m r^2 \tag{71}$$

Where r, h and m are the radius, height and mass of the cylinder.

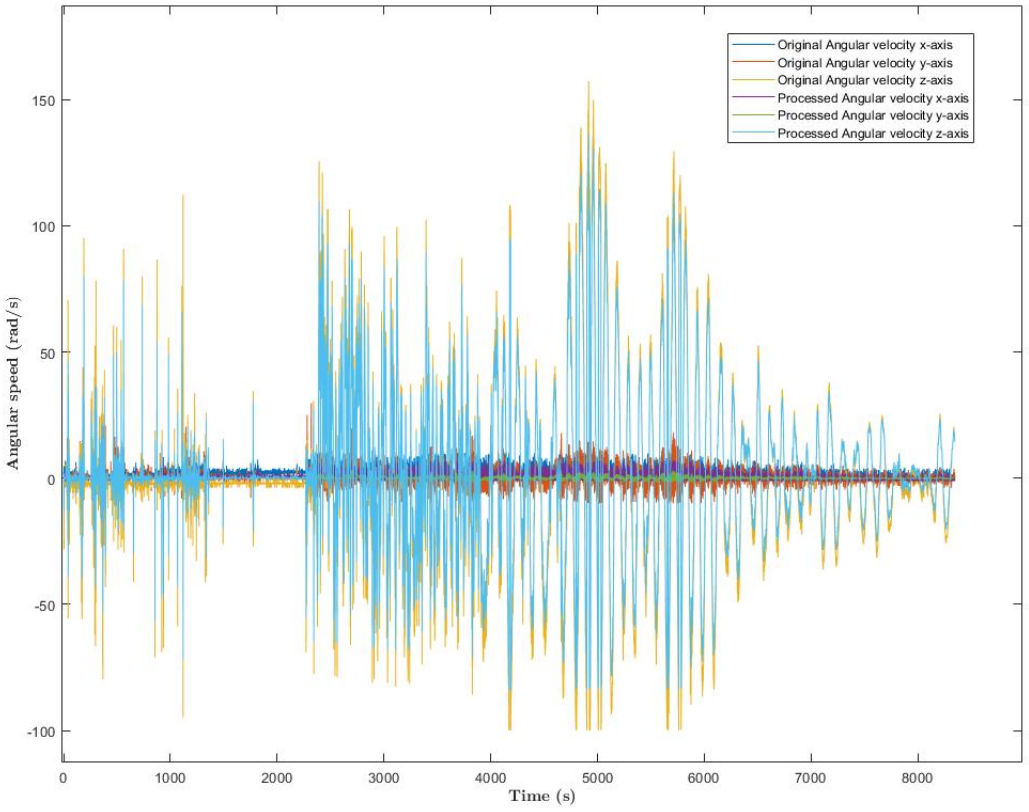

Figure 18: Comparison between the angular speed obtained by direct measurements and the processed one.

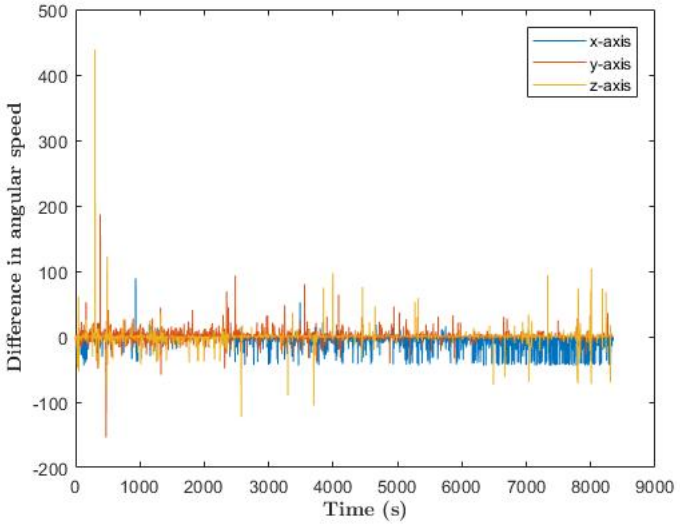

Figure 19: Difference between the original values of the angular speed and the processed ones.

On the other hand, the heavy wheel is modeled as a ringed cylinder, because of this fact the expressions employed for the calculation of the diagonal terms result to be:

$$I_x = \frac{1}{12} m \left(3 \left(r_{outer}^2 - r_{inner}^2\right) + t^2\right) \tag{72}$$

$$I_y = \frac{1}{12} m \left(3 \left(r_{outer}^2 - r_{inner}^2\right) + t^2\right) \tag{73}$$

$$I_z = \frac{1}{2} m \left(r_{outer}^2 - r_{inner}^2\right) \tag{74}$$

Where t is the thickness of the ring and r_{inner} and r_{outer} its inner and outer radius respectively and m the mass of the ring.

Since one of the sizing parameters of the wheels is density, the mass in the previous equations can be expressed as the product of the density times the volume:

$$m_{cylinder} = \rho_{cylinder} h \pi r^2 \tag{75}$$

$$m_{ring} = \rho_{ring} t \pi \left(r_{outter}^2 - r_{inner}^2\right) \tag{76}$$

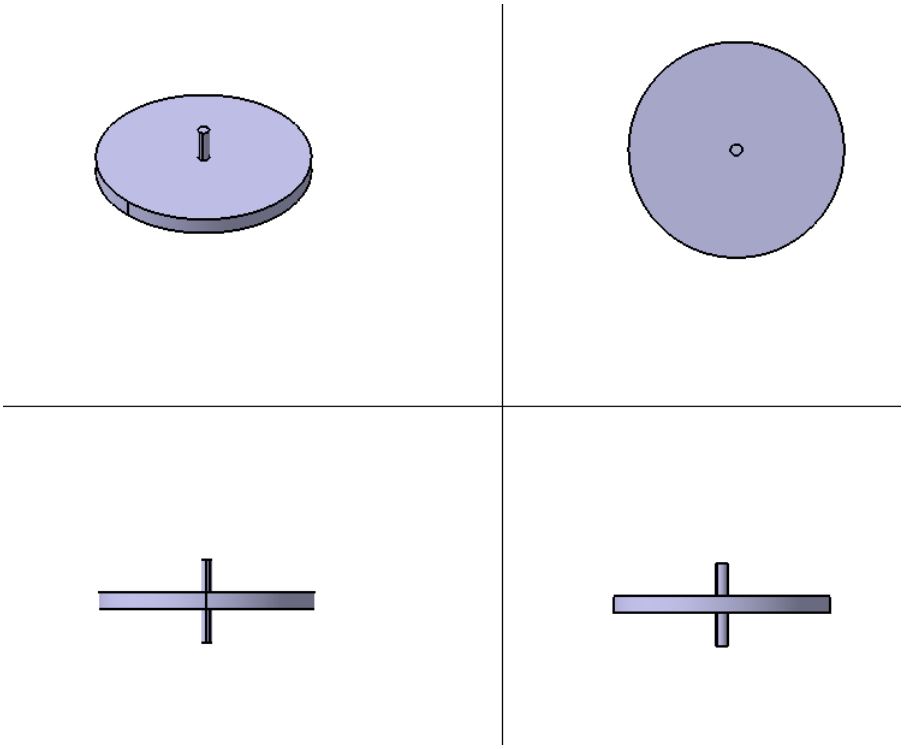

Figure 20: Base model of the compact wheel seen from different views.

Hollow wheels are very similar to the compact ones, the main different is that the inner ring is substituted by a smaller one and four connective arms that join the outer ring and the inner one as can be seen in figure 21. The tensor of inertia of this kind of wheels is the tensor of inertia of the arm, the outer ring, the smaller inner ring and the four connective arms which can be calculated by expressions (77), (78) and (79).

$$I_x = \frac{1}{12} m \left(d^2 + h^2\right) + m \left(cos\left(r\omega_{rxn} t\right)\right)^2 \tag{77}$$

$$I_y = \frac{1}{12} m \left(w^2 + h^2\right) + m \left(sin\left(r\omega_{rxn} t\right)\right)^2 \tag{78}$$

$$I_z = \frac{1}{12} m \left(d^2 + w^2\right) + mr^2 \tag{79}$$

Where d, h, and w are the depth, thickness and width respectively, and r is the distance between the center of mass of the connector and the center of mass of the structure. The thickness of the spokes is set to be the same as the one of the outer rim and its width equal to the diameter of the central hole.

The mass of each connector can be calculated as its volume multiplied by its density.

$$m_{connector} = \rho dhw \tag{80}$$

One important issue to clarify before continuing is that there are restrictions in the dimensions of the reaction wheels due to the limited space inside the gondola. As was mentioned in section 4 the prototype of gondola in which these wheels are going to be stored has an external dimensions of 22x22x19 centimeters. If the thickness of 3 centimeters of the walls is considered the internal volume turns out to be 16x16x13 centimeters. This restricts the dimensions of the reaction wheels to a maximum of 12 centimeters of diameter and 10 of thickness

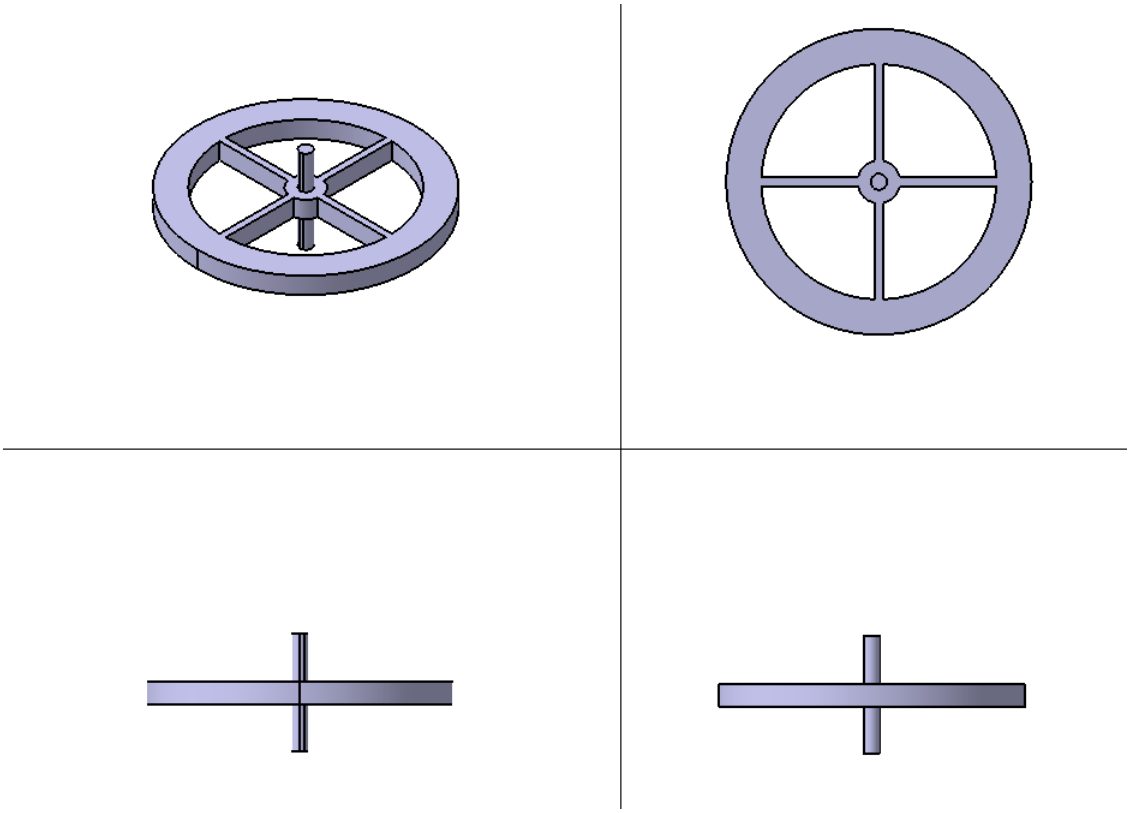

Figure 21: Base model of the hollow wheel seen from different views.

in order for a clearance with the rest of equipments to exists. Nonetheless the value of the thickness should not be larger than the diameter of the wheel for the azimuthal axis be the principal axis of the device.

The set of equations that represent the platform and the reaction wheel in the controller are (58), (59) and (46) for the determination of the attitude of the platform, and (50), (51), (52), (54), (55) and (56) for the determination of the platform's position.

However this expressions are slightly modified due to certain assumptions made in the modeling of the problem. The first assumption made is that the azimuthal axis of the reaction wheel is aligned with the one of the platform so that the tensor of inertia of the reaction wheel does not vary with time. The second assumption is that the forces acting on the z-axis are in equilibrium so that the balloon ascends or descends with constant velocity.

With these assumptions in mind expression (58) is rewritten as:

$$\frac{d\omega_{pl}}{dt} = \left(I_{rxn} + I_{pl}\right)^{-1} \left(S\left(\omega_{pl}\right) I_{pl}\omega_{pl} + I_{rxn}\left(\omega_{rxn} + S\left(\omega_{pl}\right)\omega_{rxn}\right) + S\left(\omega_{pl} + \omega_{rxn}\right) I_{rxn}\left(\omega_{pl}\omega_{rxn}+\right) - T_{ext}\right) \tag{81}$$

Where T_{ext} is the external torque induced on the platform. In order to estimate the maximum angular velocity that the reaction wheels must provide it is mandatory to also estimate the maximum amount of angular momentum that they must store. This is made by means of expression (40) using the tensor of inertia of the gondola and the data of angular velocity provided by Mexico. This is an estimation because by changing the value of the tensor of inertia the values of the angular speed induced by the external torques on the platform will also change. However, there is no data about the behavior of the gondola prototype that can be used for these calculations.

$\omega_{max}(rad/s)$	$I_{xx}(kgm^2)$	$I_{yy}(kgm^2)$	$I_{zz}(kgm^2)$	$H_{max}(kgm^2/s)$
2.4780	0.0932	0.0932	0.0189	0.05194

Table 1: Table with the maximum angular speed experimented by the gondola, tensor of inertia of the platform and the maximum angular momentum that the reaction wheel is needed to store.

From the data gathered in table 1 and the integral form of equation (57) the maximum expected angular velocity of the reaction wheel can be determined resulting expression (82).

$$w_{rmax} = I_r^{-1} \left(H - w_{pl} I_{pl} \right) \tag{82}$$

As can be appreciated in the previous equation the value of the maximum expected angular velocity depends on the tensor of inertia of the wheel. This means that the final value of the the angular velocity would decrease with increasing values of inertia. By following this expression a reaction wheel could be designed to be as heavy as possible in order to increase its tensor of inertia. Nonetheless this would suppose a significant increase in the weight of the gondola which is a key parameter that affects directly the performance of the mission and the size of the balloon that lifts the platform. Because of this reason the weight of the reaction wheel must not be greater than the 30% of the total weight of the gondola, which in this case is 0.515 kilograms.

On the other hand, if the wheel is designed to be very light the angular speed needed to store the required amount of angular momentum could shatter the device rendering useless, meaning that a trade off between weight and angular speed is needed.

In addition, a lower limit to the torque provided by the wheel must be imposed for the gondola to be able to cover a certain amount of angular units in a certain time. This can be computed as the slew torque, which is the amount of torque required for the platform to cover a certain number of angular units[10]. The slew torque can be computed by means of equation (83)[10], where T is the required torque, θ the angular units covered and t the amount of time in which those angular units are covered.

$$T = 4\theta \frac{I_{pl}}{t^2} \tag{83}$$

For the current case the required amount of angular units covered in a certain amount of time is 90 degrees each nine seconds ($\frac{\pi}{2}$ rads in 9 seconds), resulting in a required torque of $5.04 \cdot 10^{-4}$N$\cdot$ m.

The force caused by the buoyancy of the balloon is set to be equal to the weight of the platform in order to emulate the conditions of a steady flight in the azimuthal direction.

As a final comment on the simulation, three different boundaries had to be set in order to provide an accurate representation of the operational environment in which the gondola will be employed. The first one of these boundaries is to set the minimum altitude of the simulation as the ground level because in case of descend the mathematical model does not contemplate the ground level as a lower limit of in the z-direction, allowing the platform to reach negative altitudes. Following the line of the first boundary, the second one establish that if the vertical velocity of the gondola is negative (descending) and the minimum altitude is reached the platform must stop (vertical velocity set to zero) simulating a collision with the ground. The third one does not allow the balloon to fly higher than 35000 meters, in case that the balloon reach that altitude the vertical velocity would be set to zero.

5.2.5 Materials

One of the key parameters in the design of a reaction wheel is the material employed for its construction. The main parameters that are going to be taken into account are their density, their tensile strength and their price.

By inspection of the equations described above it can be deduced straightforwardly that the more massive a reaction wheel is the less angular speed it does need to develop in order to counteract the external torques applied on the gondola and correct the attitude. Nonetheless, a very heavy wheel may not be suitable for these kind of missions since they add a significant amount of mass to the whole system and they need more power to

be operated than a lighter one, which can suppose a significant reduction in the duration of a mission because of the increased power consumption.

The tensile strength of the material employed is the main parameter that determines the maximum angular velocity that the reaction wheel can reach and thus, the maximum amount of angular momentum that it can storage. The equation that determines the maximum angular speed of a ringed wheel in terms of the tensile strength of the material is the one depicted in expression (84), where ω is the angular speed of the wheel, ρ the density of the material, σ_y the yield strength of the material, ν the Poisson ratio of the material and R_o and R_i the outer and inner radius of the ring.

$$\omega = \sqrt{\frac{\sigma_y}{\frac{3+\nu}{8}\rho\left(R_o - R_i\right)^2}} \tag{84}$$

The yield strength σ is the maximum amount of load that a material can withstand deforming in an elastic way (recovering its original shape and dimensions when the load disappears). In other words, a material subjected to a load is going to deform in an elastic way until the yield strength is reached, for loads above the yield strength the material will deform plastically, being not able to recover its initial shape and dimensions.

The Poisson ratio ν is a coefficient that measures the relation between the deformation of a lineal[12] and isotropic[13] material of the longitudinal and transversal directions.

Expression (84) is can be used for the compact design since it is modeled as a ring. For the case of the hollow design expression (86) is used to to the fact that in this design the largest amount of stress is going to be concentrated in the join of the spokes with the inner ring. In this expression, A stands for the cross sectional area of the spoke and m r as the mass and radius of the spokes adding the thickness of the outer rim.

$$\sigma_y = \frac{m_s \omega_r^2 r}{A} \tag{85}$$

$$\omega = \sqrt{\frac{\sigma_y A}{mr}} \tag{86}$$

In addition to the properties described before it is important to remark that the chosen material must be corrosion resistant (or at least be coated with a layer of corrosion resistant agent) due to the fact that the inside compartments of the gondola are not isolated from the atmosphere. If the balloon encounters areas of high humidity like clouds the lifespan of the equipment can be reduced significantly. Another relevant issue is the static charge that can be generated by the spinning motion of a reaction wheel made of a electrical conductor material, in such cases an insulation coating is needed in order to avoid any damage to the rest of electronics in the platform. In addition, the rotating flywheel can generate substantial amounts of heat by friction, leading to the possible necessity of a thermal insulation jacket.

	ρ (kg/m^3)	σ_y (MPa)	ν	Approximate price (€/kg)
Aluminium 2024 T-4	2780	324	0.330	2.50
Aluminium 7075 T-6	2810	503	0.330	3.00
Titanium-6Al-4V	4430	880	0.342	30.00
Steel Aermet 340	7860	2160	0.302	18.00
ABS	1070	74	0.35	7.00
High Density Polyethylene (HDPE)	959.19	29	0.425	1.30

Table 2: Materials used for the design of the reaction wheels.

Finally, by merging equations (82) with (84)[11]-[12] and (82) with (86) two expressions that relates the required maximum amount of stored angular momentum and the maximum angular speed available for the reaction wheel before shattering can be obtained, allowing the dimensioning of both kind of wheels.

[12]Material that deforms linearly with the applied load.
[13]An isotropic material is one that shows the same structure and physical properties in all spatial directions.

The materials gathered in table 2[13, 14, 15, 16, 17, 18, 19, 20, 21, 22, 23, 24] are the ones employed in the analysis. The selection includes metals widely used in aerospace industry like heavy alloys of titanium and steel with a high yield strength, light aluminum alloys and high density polymers that can be shaped by means of 3D printing techniques.

$$\sqrt{\frac{\sigma_y}{\frac{3+\nu}{8}\rho\left(R_o - R_i\right)^2}} = \frac{H - \omega_{pl} I_{zpl}}{I_{zrc}} \tag{87}$$

$$\sqrt{\frac{\sigma_y A}{m_s r}} = \frac{H - \omega_{pl} I_{zpl}}{I_{zrh}} \tag{88}$$

Being R_o and R_i the outer and inner radius of the compact disk, m_s the mass of a stoke, r the length of the stoke accounting for the thickness of the outer rim and I_{zrc} and I_{zrh} the value of the tensor of inertia in the z-axis of the compact and outer wheel. In the case of the compact wheel the value of the inner radius is dependent of the motor in which the flywheel is connected to, while the value of the outer radius is limited by the size of the insides of the gondola (see section 5.2.4).

$$I_{zrc} = \frac{1}{2} m \left(R_{outer} - R_{inner}\right)^2 \tag{89}$$

$$I_{zrh} = \left[\frac{1}{12} m \left(d^2 + w^2\right) + m \left(\frac{d}{2} + r_{outer}\right)^2 + \frac{1}{2}\left(m_i \left(R_{i_{outer}} - R_{i_{inner}}\right)^2 + \left(m_o \left(R_{o_{outer}} - R_{o_{inner}}\right)^2\right)\right)\right] \tag{90}$$

As a final remark it is of paramount relevance to clarify that the whole wheel in both kind of designs is made of the same material, with the same properties such as density, young modulus or Poisson's ratio.

5.2.6 Controller

As was mentioned before a controller was implemented in the simulation in order to model the control system that the gondola may have installed in the future. The constants of the controller were chosen regarding the values of three parameters: Rise time, settling time and overshoot

- The rise time is the time time it takes for the response to rise from 10% to 90% of the commanded value.
- The settling time is the time it takes for the error to reach a value that only differs ±2% of the commanded value in the steady state.
- The overshoot is the percentage that the peak exceed the commanded value

The desired values of the aforementioned parameters are gathered in table 3

Rise time (s)	Settling time (s)	Overshoot
1	2	0.2

Table 3: Desired values of the main signal parameters.

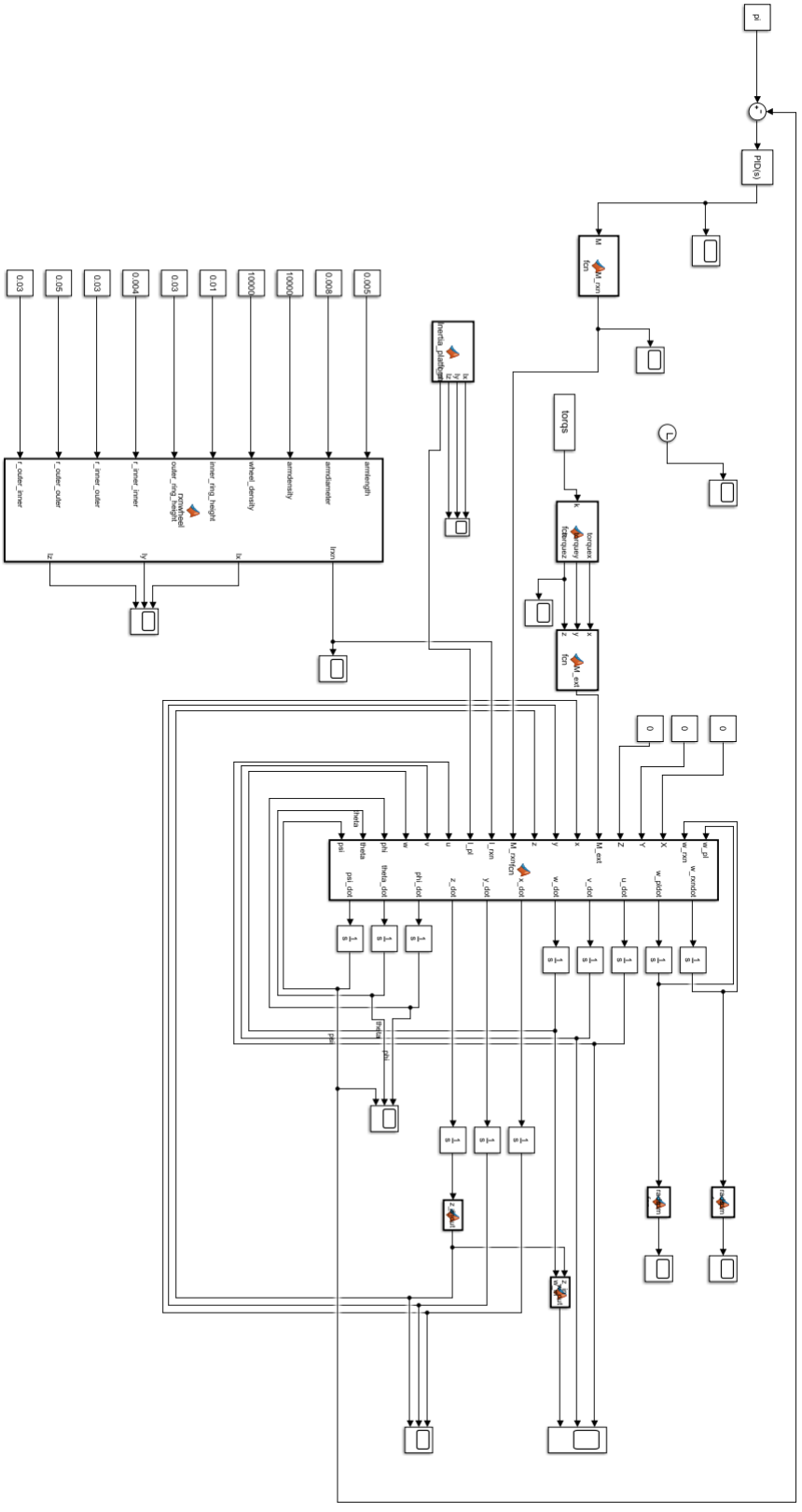

Figure 22: Simulink model of the simulation for testing the distinct models of reaction wheels.

6 Results

First of all, the simulation was tested on the platform used by National Institute of Technology of Mexico which consisted on a prismatic platform with an upper prism attached as can be seen in figure 23 with a total mass of 2.7 kilograms. The main goal of this simulation is to confirm the consistency of the model by checking the relation between the variables involved, i.e. if a large variation in the torque induced in the gondola appears, a large variation in its angular velocity and the one of the reaction wheel is expected, as well as a sudden variation in the attitude of the platform.

As can be appreciated in figures 24 and 25 four different regions can be appreciated: A first one with pronounced peaks that leads to a second one more stable, a third one in which three large peaks are present and finally another stable region. This mentioned sectors match with the ones seen in the torque spectrum used depicted in figure 15.

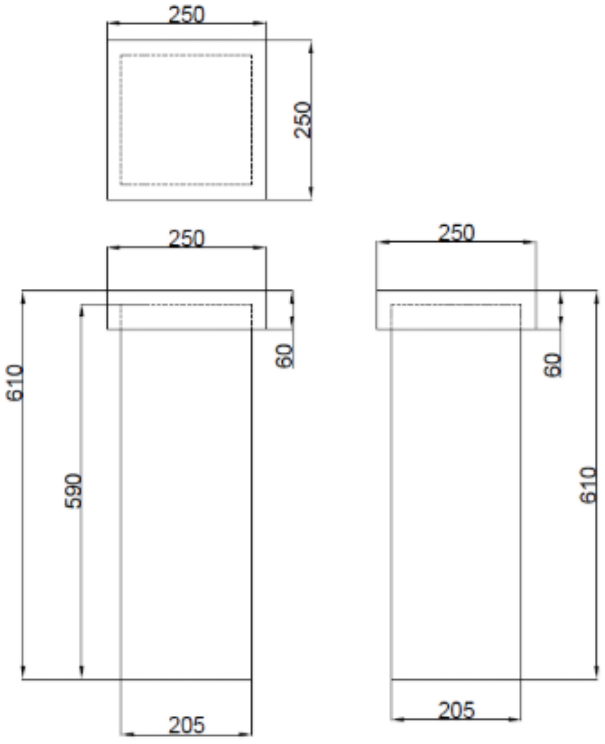

Figure 23: Gondola employed for the measurement of the initial data (units in millimeters).

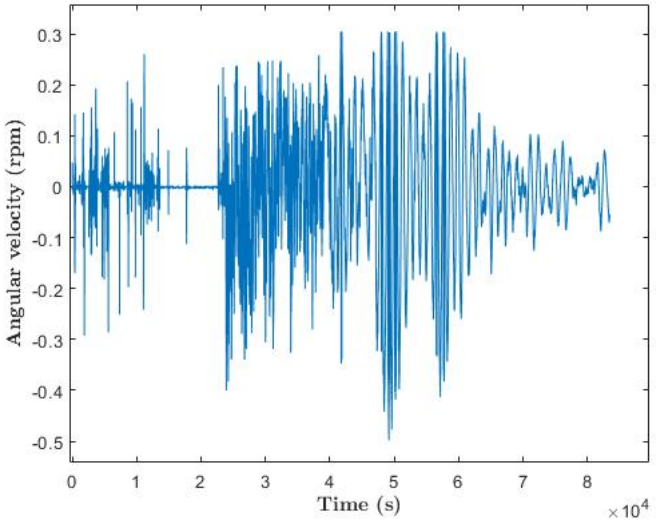

Figure 24: Angular velocity of the gondola about the z-axis.

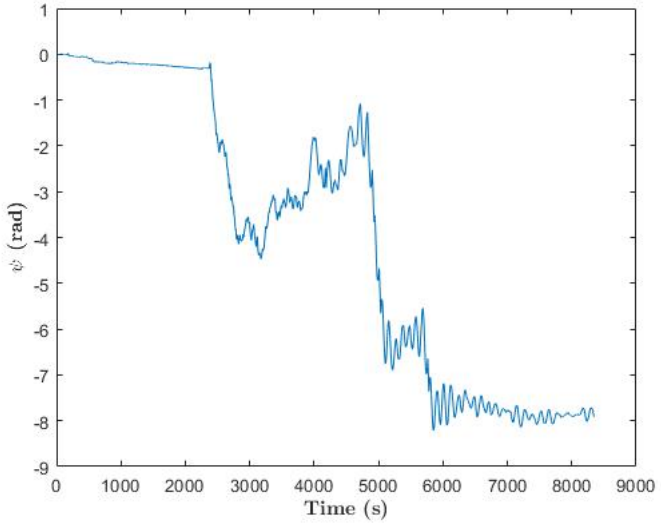

Figure 25: Evolution of the azimuthal angle in time uncontrolled.

The values of the constants used in the PID controller implemented on the model used for this test can be seen in table 4.

Once the validation test was performed on the gondola used for the data gathering a "dummy" wheel was implemented in order to test the reliability of the controller in the simulation. The values of the constat of the controller can be seen in table 4, while the main parameters of the reaction wheel are gathered in table 5.

Proportional	Integral	Derivative
-0.5	-0.1	-1

Table 4: Values employed for the three different constants in a PID

	Arm	Inner ring	Outer ring	
Density (kg/m^3)	8000	8000	8000	
Diameter(m)	0.008	0.050	0.050	
Thickness (m)	0.050	0.010	0.010	Total mass (kg)
Mass (kg)	0.002	0.222	1.206	1.430

Table 5: Specifications of the reaction wheel used for the test of the controller.

In figures 26, 28 and 27 the same four regions appears. In addition, the action of the controller is appreciated changing the initial state of the azimuthal angle to the commanded one in less than a second (from 0° to 90°). In figure 28 it is important to highlight how the gondola rotates at an angular velocity close to 0 most of time. This is the result of the rotation of the reaction wheel that exchanges momentum with the platform in order to correct the attitude.

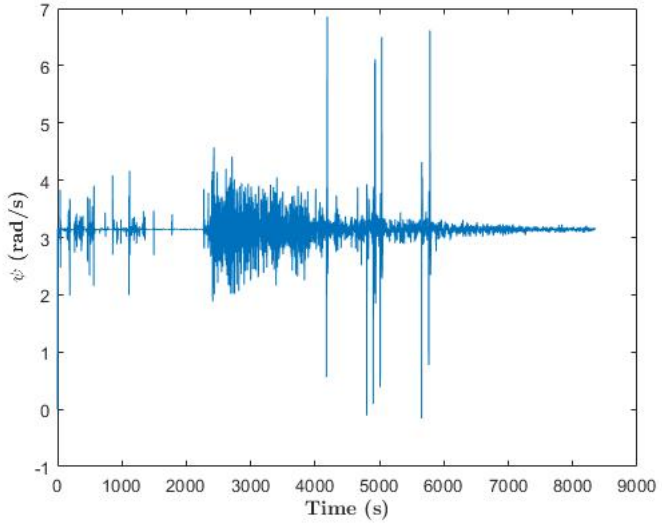

Figure 26: Evolution of the controlled azimuthal angle with time.

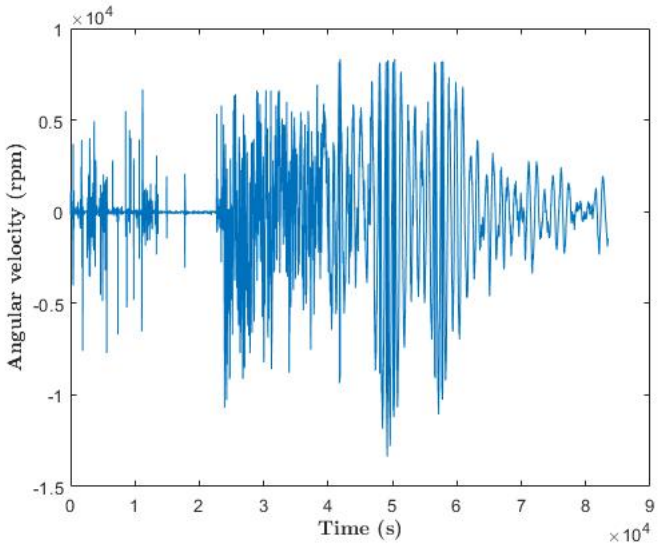

Figure 27: Evolution in time of the angular velocity of the reaction wheel.

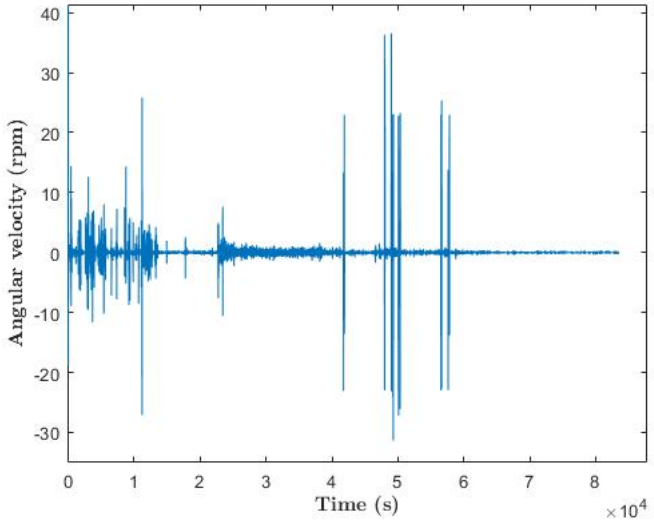

Figure 28: Evolution of the controlled angular velocity of the gondola with time.

6.1 Compact wheels

For the compact flywheel the inner radius is set to 3 millimeters as is a common value of motor shaft's case hole, while the external radius is set to the maximum available of 6 centimeters.

	$\omega_{max}(rpm)$	$I_z(kgm^2 \cdot 10^{-6})$	Thickness $(m \cdot 10^{-5})$	Mass (g)
Aluminium 2024 T-4	8.865E4	3.860	6.855	2.1
Aluminium 7075 T-6	1.100E5	3.115	5.472	1.7
Titanium-6Al-4V	1.155E5	2.962	3.301	1.6
Steel Aermet 340	1.367E5	2.503	1.572	1.4
ABS	6.808E4	5.026	23.189	2.8
High Density Polyethylene (HDPE)	4.452E4	7.686	39.559	4.3

Table 6: Table with the maximum possible angular velocity of the flywheels and the values of the moment of inertia, thickness and mass needed to store the maximum required angular momentum at that speed.

As can be seen in table 6 at the maximum rotational speed of this kind of flywheel the required moment of inertia and thus the resultant mass and thickness of the wheels are very small. This is certainly an advantage because it allows to manufacture small light wheels that do not suppose a significant increase of the mass of the system. Nonetheless making a wheel rotate at these speeds may consumer large amounts of power and can generate levels of temperature due to friction that the components may not be able to withstand, (for instances, ABS plastics have a melting point around 200°C). For these reasons an upper limit to the maximum velocity must be set. For many reaction wheels and DC motors that can be found in the market this limit in the angular speed is between 10000 and 60000 revolutions per minutes. For this analysis an intermediate value of 8000 revolutions per minute would be used.

Then, the moment of inertia, thickness and mass required is recalculated for this value of the maximum angular velocity resulting in the values that can be seen in table 7.

	$I_z(kgm^2 \cdot 10^{-5})$	Thickness (mm)	Mass (g)	Price (cents of €)
Aluminium 2024 T-4	4.277	0.760	23.800	5.95
Aluminium 7075 T-6	4.277	0.752	23.800	7.14
Titanium-6Al-4V	4.277	0.477	23.800	71.40
Steel Aermet 340	4.277	0.269	23.800	42.84
ABS	4.277	2.000	23.800	16.67
High Density Polyethylene (HDPE)	4.277	2.200	23.800	3.09

Table 7: Moment of inertia, thickness, mass and price of the reaction wheels.

As was expected, once the value of the rotational speed is fixed the moment of inertia of all the wheels remains constant. A remarkable result is that the mass is the same in all the flywheels. This is because all the parameters of the moment of inertia are set to be constant except for the density and the thickness and, since the moment of inertia has to be the same, this two values compensate giving as a result the same value for the mass.

In addition, it must be highlighted that the values of the thickness allows to reduce the value of the maximum radius. Despite these values of the mass being very low, this thickness is very difficult to obtain in the manufacturing process. Furthermore, a flywheel with those values of thickness is very prone to break up if hit by any component of the gondola that goes out of place.

In order to check the evolution of the thickness with the value of the outer radius of the disk a plot of both variables was performed.

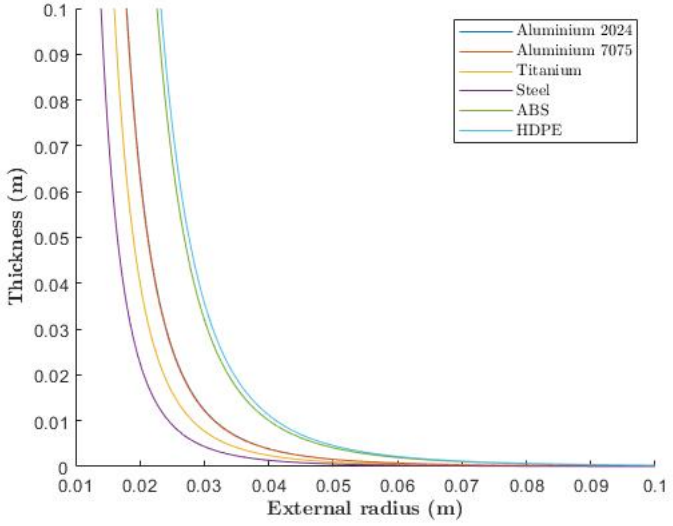

Figure 29: Evolution of the thickness with the outer radius

As can be seen in figure 29 the values of the thickness decrease exponentially with decreasing values of the outer radius. It is important to mention that in the range between 3 and 4 centimeters of external radius values between 0.3 and 3.6 centimeters can be found which fit in the range of dimensions suitable for this gondola.

In table 8 the values of the thickness for an outer radius of 3cm vary between 0.440 and 3.580 centimeters, having a moment of inertia of $4.2255 \cdot 10^{-5} kg/m^2$ and a mass of 96 grams they suppose only a 5.6% of the total mass of the gondola, falling withing the range of the required mass.

	Thickness (cm)	Price (cents of \euro)	Mass (g)
Aluminium 2024 T-4	1.230	24.00	96.00
Aluminium 7075 T-6	1.220	28.80	96.00
Titanium-6Al-4V	0.770	288.00	96.00
Steel Aermet 340	0.440	172.80	96.00
ABS	3.210	67.20	96.00
High Density Polyethylene (HDPE)	3.580	12.48	96.00

Table 8: Thickness, mass and prices of the reaction wheels.

As was mentioned before, the heaviest materials result in a thinner flywheel. However, these are also the most expensive. In the case of titanium an increase of ten times the cost with respect the second aluminum allows a reduction in thickness of 58%. In the case of steel the reduction of thickness reaches a 177% with a cost of five times the aluminum wheel. The polymers present lower price than the heavy metals. However, they are much thicker and the ABS one is still more expensive than the ones made of aluminum.

Then, the wheel with this inertia was implemented in the simulation in order to test its performance, resulting in the data plotted in figures 30, 31 and 32. The controller used for this wheel to accomplish the requirements of rise time, settling time and overshoot are the ones depicted in table 9, being these variables 0.8s, 1.9s and 5%.

Proportional	Derivative	Integral
-0.5	-0.1	-0.1

Table 9: Values of the constants of the PID

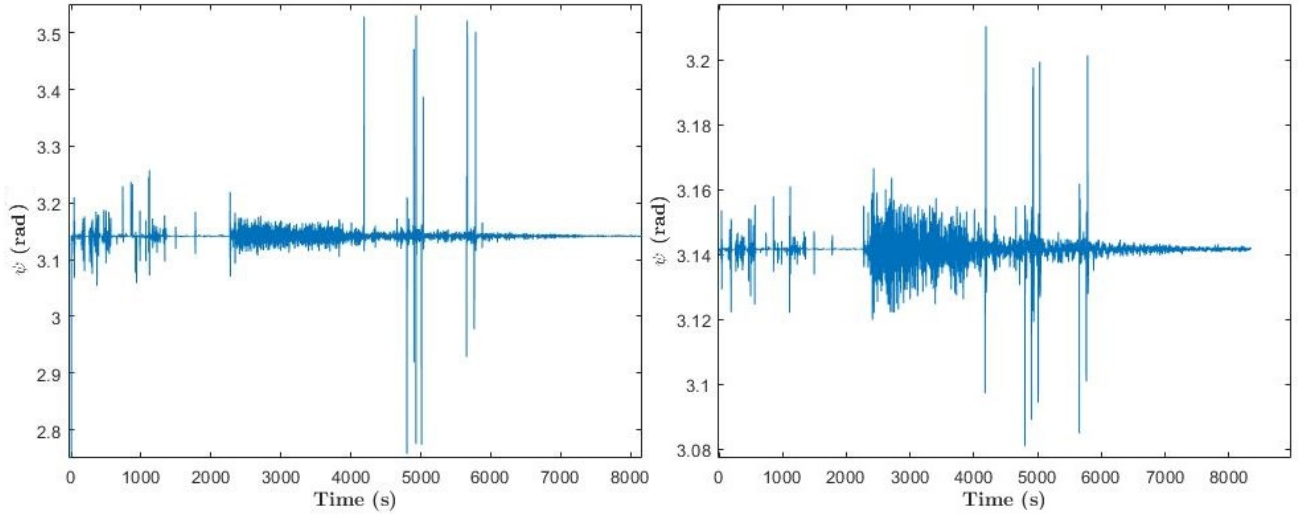

Figure 30: Evolution of the azimuthal angle with time. At left with a commanded value of π from an initial angle of 0^o. At right, with an initial value of π.

The commanded value for the azimuthal angle is 90 degrees being 0 degrees the initial position. The initial values of the angular velocity of the platform and the reaction wheel are 50 and -200 rpm respectively. At first glance, the wheel seems to perform adequately. However, by taking a closer look to figure 32 it can be appreciated that the angular speed exceeds the limit of 8000 rpm imposed before. This is thought to be caused by the difference between the inertia of the platform used to gather data (which was calculated roughly with not enough data) and the one of the gondola prototype.

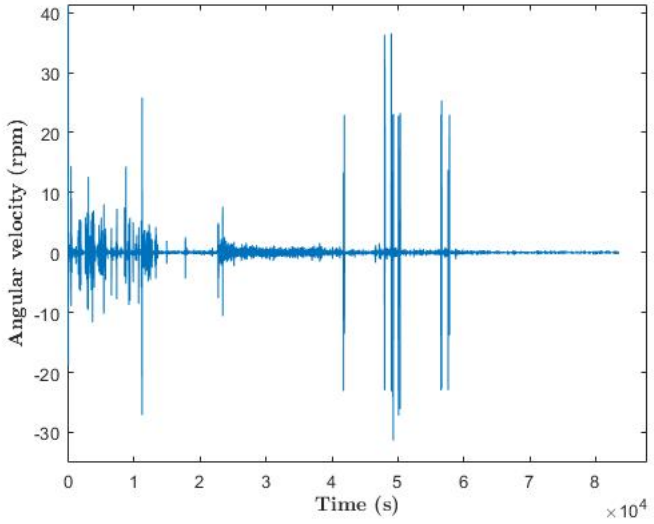

Figure 31: Evolution of the angular speed of the gondola with time

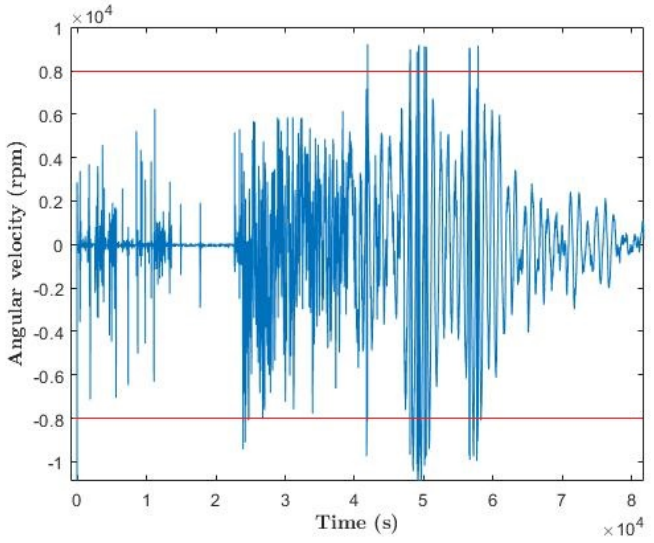

Figure 32: Evolution of the angular velocity of the reaction wheel with time. In red it is marked the saturation speed of 8000 rpm.

6.2 Hollow wheels

In order to make a fair comparison between both kind of wheels the same external radius, inner hole, maximum angular velocity and inertia were chosen for the analysis.

Since a hollow wheel with the same external radius and thickness would have less amount of material than a compact one, it means that it would also have a reduced moment of inertia in the z-axis.

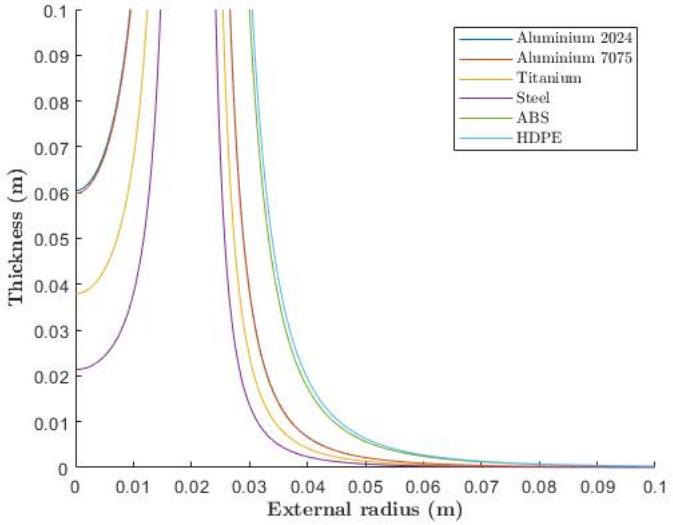

Figure 33: Variation of wheel thickness with the external radius in hollow wheels.

	Thickness (cm)	Price (cents of \euro)	Mass (g)
Aluminium 2024 T-4	3.871	59.75	239.00
Aluminium 7075 T-6	3.833	71.70	239.00
Titanium-6Al-4V	2.429	717.00	239.00
Steel Aermet 340	1.369	430.20	239.00
ABS	10.056	167.30	239.00
High Density Polyethylene (HDPE)	11.222	31.07	239.00

Table 10: Thickness, mass and prices of the hollow designs.

In table 10 it can be seen that the values of the thickness are larger than the ones of the compact flywheel as was predicted before. As a result, the mass of the wheel has been increasing to a value of 0.239 kilograms supposing an increase of 249% in weight. Nonetheless, the metallic materials steel offer acceptable values for the thickness that fall in the limits of the requirements for the gondola prototype. In addition, the mass suppose only a 14% of the total mass of the gondola, allowing the possible implementation of this kind of design.

In terms of costs the situation is pretty much the same as with the compact flywheels. The heavy alloys provide the smallest thickness and the polymers the largest. In both models aluminum wheels are the ones that provide the best relation between thickness and prices, being Aluminium 2024 T-6 the most suitable since in only supposes an increase of a 1% in thickness with a decrease of a 20% in price.

7 Conclusions

Within this document the preliminary sizing process of a reaction wheel for a prototype of high altitude platform consisting of a gondola and a helium balloon has been performed. In order to do so many branches of physics has been involved such as classical mechanics, structural dynamics and data processing. The hearth of the project was always around the kinematics and dynamics of rotors and its physical properties such as their moment of inertia or structural properties.

The principal kind of reaction wheel developed along this document has been a solid disk with a small shaft in the middle that allow it to be connected to a DC. In addition, it has been compared to an alternative design consisting in a rim connected to the same shaft by four connectors or spokes.

In order to model the dimensions of the flywheel the equations for the shattering speed of both kind of designs have been used, but slightly modified in order to account for the speed at which they would start deforming plastically instead of doing it in an elastic way.

In order to test the effectiveness of the designs a simulation that resembles the conditions that the attitude control system would encounter in real life operations was developed. To do that, equations of classical mechanics concerning rotatory bodies were implemented in MATLAB and Simulink. In addition, the data employed to model forces and torques the system would be subjected to in a real life scenario was, in fact, real data obtained from a sub orbital flight in very similar conditions to the ones that the platform would experience in a nominal mission. However, this data was collected by a system with certain differences in mass and geometry with the one in which the reaction wheel is going to be implemented, resulting in a certain degree of error in some parameters of the simulation.

For the design of the wheel 6 different materials have been considered, 4 of them were metals widely used in the aerospace industry and the other two were polymers used in 3D printing. As was expected, the metals with higher density allowed the use of smaller and lighter reaction wheels while the plastic ones required of much more volume to be as effective as the metallic ones.

Regarding of which of both models is more suitable it turned out that the solid design allowed the implementation of smaller and lighter wheels than the model with spokes. However, it is of paramount importance to mention that the study was performed taking into account that the whole flywheel was made of the same material. It could be possible to develop a spoke model in which the connectors were made of a light component with a very high traction resistance like a carbon fiber composite, while the outer rim could be made of a very dense material like lead of tungsten that showed similar or better results that the ones achieved by the compact design. This could be work for later investigation.

In terms of costs and size, the wheels made of heavy alloys allow the selection of thinner wheels than aluminum and polymer wheels. However these are much more expensive than the other ones despite their significant reduction in thickness. In terms of efficiency, the aluminium wheels are the ones that offer the best trade between cost and thickness, in particular the one made of Aluminium 2024 T-4.

A Regulatory framework

In appendix 2.5 of SERA[25] (regulatory framework of airspace and common operative rules for services and procedures of air navigation) establishes that an unmanned and uncontrolled balloon is classified in three subgroups:

- **Light**: Unmanned and uncontrolled balloon that bears an operative payload of less than 4 kg.
- **Medium**: Unmanned and uncontrolled balloon that bears an operative payload of less than 6 kg.
- **Heavy**: An unmanned and uncontrolled balloon is considered heavy if:
  - It bears an operative payload of 6kg or larger.
  - It carries an independent part of its payload of larger.
  - An independent part of its payload is of 2kg or more and has a density of more than 13 g/cm^2.
  - It employs a rope or other element used to hold in suspension the operative payload with an impact force of 230N required to separate the suspended operative payload.

It also contemplates the general rules of employment.

- Any unmanned and uncontrolled balloon could be employed without the proper authorization of the state from which it is launched
- Any unmanned and uncontrolled balloon that does not fall in the category of light balloons with meteorological goals employed with authorization of the competent authority would be employed over the aerial space of other state without its authorization.
- The authorization for the employment of the balloon must be obtained before the launch if probabilities of crossing the airspace of other state exist.
- All unmanned and uncontrolled balloons will operate under the established regulations of the state over they fly.
- An unmanned and uncontrolled balloon which its fall or the fall of any of its components may suppose any risk to people or goods not related with the operation of the balloon will not be allow to operate.
- A heavy unmanned and uncontrolled balloon will not be allow to operate over the sea without any previous coordination with the navigation services providers.

In addition, the limitations of usage and equipment requirements are contemplated:

- No heavy unmanned and uncontrolled balloon would operate without the previous authorization of the navigation services provider, at a level of pressure altitude inferior of 18000m in which:
  - There are more than 4 oktas of clouds.
  - The horizontal visibility is inferior to 8km.
- Any medium or heavy unmanned and uncontrolled balloon must not be launch if it is likely to fly under an altitude of 300m over urbanized areas or people exposed to impact that are not related with the operation of the balloon.
- A heavy unmanned and uncontrolled balloon may not operate unless:
  - It is equipped with a minimum of two devices independent of each other to interrupt the flight that are activated remotely.
  - If the balloon is made of polyethylene and of null pressurization, two different ways of interrupting the flight are needed.
  - The balloon has a recovery that reflects RADAR signals in the spectrum between 200MHz to 2700MHz, or the balloon is equipped with devices that allow its continuous location from ground.

- Heavy unmanned and uncontrolled balloons must not operate under the following conditions:
  - Over areas where an SSR based equipment on ground, unless the balloon is equipped with a secondary radar transponder with capacity of notifying the pressure altitude that works continuously in an assassinated call sign, or when its needed, the ground station can put to work.
  - In areas where an equipment ADS-B based on ground unless the balloon is equipped with a transmitter ADS-B with capacity of notifying the pressure altitude that is continuously active or it can be activated from ground when needed.
- Heavy balloons with holding systems that require a force larger than 230N to break up wont be allowed to fly unless they have colorful indicators located in intervals not larger than 15m
- Balloons flying at a pressure altitude smaller than 18000m will not be allowed to fly between the sunset and the sunrise unless they are properly lighted.
- Heavy balloons with suspension equipment like parachutes larger than 15m long will not be allowed to fly between the sunset and the sunrise at a pressure altitude inferior to 18000m unless that suspension equipment is properly lighted.

It is also contemplated that the flight interruption devices for heavy balloon must be activated when:

- The meteorological conditions wont satisfy the stipulated conditions for the operation.
- An imperfection or any reason that would turn the operation into a hazard to air traffic or to the people or goods on ground.
- Entering the airspace of another state without permission.

A previous notification of the operation of a medium or heavy unmanned and uncontrolled balloon to the authorities of services of air traffic with a period of at least 7 days before the flight must be effectuated.

The notification must include the following terms:

- The flight identification.
- Classification and description of the balloon.
- The SSR code, airship address or NDB frequency.
- Name and telephone number of the balloon operator.
- Location from where the balloon is launched.
- Hour of launch.
- Number of balloons that are going to be launched and the interval between each launch.
- Predicted ascension trajectory.
- Pressure altitude of cruise.
- Time to cross the 18000m line since the moment of launch.
- Hour and date of the ending of the flight

Any modification of the information notified must be communicated with 6 hours of anticipation to the dependency of air traffic services from the launch time. In case of cosmic events, these modifications must be communicated with 30 minutes of anticipation.

Once the balloon has been launched the following information must be communicated to the dependency of air traffic services:

- Identification of the balloon.
- Location where the launch took place.
- Effective time of the launch.

- Time at which the balloon is expected to cross the 18000m pressure altitude line.
- Any modification of the information previously communicated.

In case of cancellation of the flight the operator must communicate that information to the dependency of air traffic services as soon as possible.

B Project budget

This project was developed between the forth week of January and the third week of June, working an approximate of 3 hours per and 5 days per weeks during 23 weeks make up a total of 345 hours, which can be translated to 14-12 ETCS credits[14][26]. To that time it must be added the time that the student spent in tutorships and other activities involved which can add to a total of 13 hours, supposing a total of 358 hours. Taking into account that the approximate salary of a junior engineering is around 20 €per hour makes up a workforce cost of 7160 €. In addition a computer with an academic MATLAB license was needed to develop all these task supposing a cost of 900 and 500 €respectively. In addition, in order to attend to the tutorships and the other activities related with the development of the project that did not take place near the working environment of the student, he had to expend 20 €per month in public transport supposing an additional cost of 100 €. The total cost of the project is gathered in tables 11, 12 and 13 that is depicted before.

	Cost (€)
Direct labor	6900
Other tasks	260
Transportation	100
Total	7260

Table 11: Labor related costs.

	Cost (€)
Computer	900
MATLAB license	500
Total	1400

Table 12: Cost related with the means of production.

	Cost (€)
Labor related costs	7260
Means of production related costs	1400
Total	8660

Table 13: Total costs.

[14] An ETCS credit is a unit of measurement of the amount of time that an student dedicates to a certain subject or task. An ETCS credit is equivalent to 25-30 hours of dedication. It includes the the time dedicated to lectures, hours of study, tutorships, seminars, projects, learning jobs in companies and time of preparation of exams and evaluations.

References

[1] ATK. *Constellation Second Orion Launch Abort System Attitude Control Motor Ground Test*, 2010. https://www.nasa.gov/mission_pages/constellation/multimedia/orion_acm_test2.html [Accessed:17-05-2018].

[2] Ad Meskens. *Antwerp V-2.jpg*, 2009. https://commons.wikimedia.org/wiki/File:Antwerp_V-2.jpg [Accessed:10-06-2018].

[3] NASA Ames / Dana Berry. *LADEE Fires Thrusters Artist's Concep*, 2013. https://solarsystem.nasa.gov/resources/269/ladee-fires-thrusters-artists-concept/ [Accessed:3-03-2018].

[4] NN Gandilo, PAR Ade, M Amiri, FE Angilè, SJ Benton, JJ Bock, JR Bond, SA Bryan, HC Chiang, CR Contaldi, et al. Attitude determination for balloon-borne experiments. In *Ground-based and Airborne Telescopes V*, volume 9145, page 91452U. International Society for Optics and Photonics, 2014.

[5] Peter Fortescue, Graham Swinerd, and John Stark. *Spacecraft systems engineering*. John Wiley & Sons, 2011.

[6] Ashish Tewari. *Atmospheric and space flight dynamics*. Springer, 2007.

[7] Bernard Etkin and Lloyd Duff Reid. *Dynamics of flight: stability and control*, volume 3. Wiley New York, 1996.

[8] Jack A Myers. Handbook of equations for mass and area properties of various geometrical shapes. Technical report, NAVAL ORDNANCE TEST STATION CHINA LAKE CA, 1962.

[9] Espen Oland and Rune Schlanbusch. Reaction wheel design for cubesats. In *Recent Advances in Space Technologies, 2009. RAST'09. 4th International Conference on*, pages 778–783. IEEE, 2009.

[10] Wiley J Larson and Linda K Pranke. *Human spaceflight mission analysis and design (spacetechnology Series)*. New York: McGraw?Hill, 1999.

[11] Nisbett.K Budynas.R. *higley's Mechanical Engineering Design . 10th edition*. McGraw?Hill, 2014.

[12] Budynas.R Young.W.C. *Roark's Formulas for Stress and Strain, 8th Edition*. McGraw?Hill, 2011.

[13] alibaba. *Aluminium 2024 price per kilogram*, 2018. https://spanish.alibaba.com/g/2024-aluminum-price-per-kg.html [Accessed:10-06-2018].

[14] alibaba. *Aluminium 7075 price per kilogram*, 2018. https://spanish.alibaba.com/g/aluminium-7075-price-per-kg.html [Accessed:10-06-2018].

[15] alibaba. *Titanium-6Al-4V price per kilogram*, 2018. https://www.alibaba.com/showroom/titanium-ti-6al-4v.html [Accessed:10-06-2018].

[16] 2innovativesteel. *High strength low cost steel*, 2018. https://www.2innovativesteel.net/what-we-do/high-strength-low-cost-steel/ [Accessed:10-06-2018].

[17] plastemart. *polymer pricelist*, 2018. http://www.plastemart.com/polymer-pricelist/hdpe-reliance/2/9 [Accessed:10-06-2018].

[18] Aerospace Specification Metals Inc. *Aluminum 2024-T4; 2024-T351"*, note =.

[19] Aerospace Specification Metals Inc. *Aluminum 7075-T6; 7075-T651*, 2018. http://asm.matweb.com/search/SpecificMaterial.asp?bassnum=ma7075t6 [Accessed:10-06-2018].

[20] MatWeb. *Carpenter AerMet? 340*, 2018. http://www.matweb.com/search/datasheettext.aspx?matguid=64583c8ce6724989a11e1ef598d3273d [Accessed:10-06-2018].

[21] Aerospace Specification Metals Inc. *Titanium Ti-6Al-4V (Grade 5), Annealed*, 2018. http://asm.matweb.com/search/SpecificMaterial.asp?bassnum=mtp641 [Accessed:10-06-2018].

[22] Engineeringtoolbox.com. *Thermoplastics - Physical Properties*, 2018. https://www.engineeringtoolbox.com/physical-properties-thermoplastics-d_808.html [Accessed:11-06-2018].

[23] Plastics International. *High Density Polyethylene*, 2018. https://www.plasticsintl.com/datasheets/HDPE.pdf [Accessed:11-06-2018].

[24] platts. *HDPE price*, 2018. https://www.platts.com.es/news-feature/2016/petrochemicals/global-polymer-pricing-analysis/hdpe [Accessed:10-06-2018].

[25] SERA. *Reglamento de ejecuci?n (UE) No 923/2012 de la comisi?n de 26 de septiembre de 2012*, 2012. https://www.seguridadaerea.gob.es/media/4342634/regl_ue_923_2012.pdf [Accessed:10-06-2018].

[26] UNED. *Creditos Europes ETCS*, 2018. http://portal.uned.es/portal/page?_pageid=355,3138322&_dad=portal [Accessed:10-06-2018].